Title

Virus transport from drywells under constant head conditions: A modeling study

Authors

Sasidharan, Salini
Bradford, Scott A
Šimůnek, Jiří
et al.

Publication Date

2021-06-01

DOI

10.1016/j.watres.2021.117040

Peer reviewed

Published in final edited form as:
Water Res. 2021 June 01; 197: 117040. doi:10.1016/j.watres.2021.117040.

Virus Transport from Drywells Under Constant Head Conditions: A Modeling Study

Salini Sasidharan[1,2,*], **Scott A. Bradford**[2], **Jiří Šimůnek**[1], **Stephen R. Kraemer**[3]

[1]Department of Environmental Sciences, University of California, Riverside, CA 92521, USA

[2]United States Department of Agriculture, Agricultural Research Service, Sustainable Agricultural Water Systems Unit, Davis, CA 95616, USA

[3]U.S. Environmental Protection Agency, Office of Research and Development, San Francisco, CA 94105

Abstract

Many arid and semi-arid regions of the world face challenges in maintaining the water quantity and quality needs of growing populations. A drywell is an engineered vadose zone infiltration device widely used for stormwater capture and managed aquifer recharge. To our knowledge, no prior studies have quantitatively examined virus transport from a drywell, especially in the presence of subsurface heterogeneity. Axisymmetric numerical experiments were conducted to systematically study virus fate from a drywell for various virus removal and subsurface heterogeneity scenarios under steady-state flow conditions from a constant head reservoir. Subsurface domains were homogeneous or had stochastic heterogeneity with selected standard deviation (σ) of lognormal distribution in saturated hydraulic conductivity and horizontal (X) and vertical (Z) correlation lengths. Low levels of virus concentration tailing can occur even at a separation distance of 22 m from the bottom of the drywell, and 6-$\log_{10}$ virus removal was not achieved when a small detachment rate $\left(k_{d1} = 1 \times 10^{-5} \text{min}^{-1}\right)$ is present in a homogeneous domain. Improved virus removal was achieved at a depth of 22 m in the presence of horizontal lenses (e.g., X=10 m, Z=0.1 m, σ=1) that enhanced the lateral movement and distribution of the virus. In contrast, faster downward movement of the virus with an early arrival time at a depth of 22 m occurred when considering a vertical correlation in permeability (X=1 m, Z=2 m, σ=1). Therefore, the general assumption of a 1.5–12 m separation distance to protect water quality

*Corresponding Author Salini Sasidharan, USDA, ARS, Salinity Laboratory, Riverside, CA 92507, United, States, Phone: +951-369-4823, salinis@ucr.edu.

AUTHOR CONTRIBUTION

1. Salini Sasidharan: Investigation, Methodology, Software, Formal Analysis, Validation, Data Curation, Writing - Original Draft, Visualization
2. Scott A. Bradford: Conceptualization, Software, Resources, Writing - Review & Editing, Supervision, Project Administration
3. Jiří Šimůnek: Conceptualization, Software, Resources, Writing - Review & Editing, Supervision, Project Administration
4. Stephen R. Kraemer: Writing - Review & Editing, Project Administration, Funding Acquisition

Competing Financial Interest
None.

SUPPLEMENTARY MATERIAL
S1.METHOD, S1.1. Selection of Input Parameters, S1.2. Stochastic Heterogeneity and S2. FIGURES S1 (observed and fitted BTC for virus PRD1), S2 (imported pressure head, homogeneous), S3 (virus BTC explanation), S4 (velocity distribution), S5 (in-situ iron oxide treatment), S6 (virus removal), S7 (imported pressure head, heterogeneous), S8 (arrival time), and S9 (point vs. integrated virus concentration) are given in the Supplementary Document.

may not be adequate in some instances, and site-specific microbial risk assessment is essential to minimize risk. Microbial water quality can potentially be improved by using an in situ soil treatment with iron oxides to increase irreversible attachment and solid-phase inactivation.

Graphical Abstract

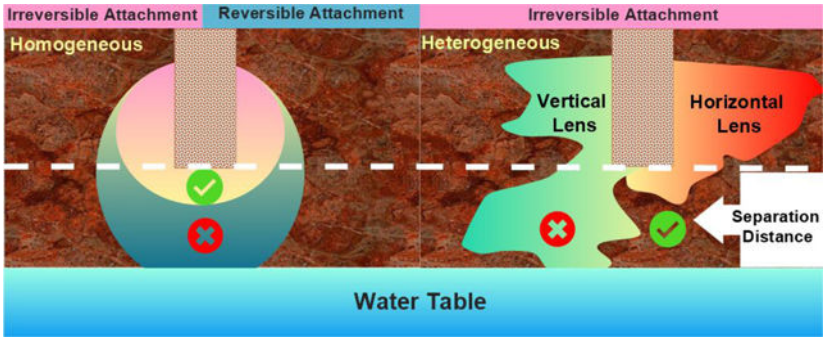

Keywords

Vadose Zone; Managed Aquifer Recharge; Drywell; Virus; Water Quality; HYDRUS (2D/3D)

1. INTRODUCTION

Groundwater is the primary source of freshwater supplies to billions of people worldwide (Gleeson et al. 2012, Taylor et al. 2013). However, microbiological contamination of groundwater (Feighery et al. 2013, Gunnarsdottir et al. 2013, Kauppinen et al. 2018, Pitkänen et al. 2011, Powell et al. 2003) causes waterborne disease outbreaks worldwide and is a growing problem in the United States (Barwick et al. 2000, Dowd et al. 1998, Fong et al. 2007, Keswick 1980, Levy et al. 1998). Sixty-four percent of the drinking water diseases between 1989 and 2002 in the U.S. were related to microbially contaminated groundwater (Fong et al. 2007). According to the World Health Organization, contaminated drinking water can transmit diseases that are estimated to cause 485,000 diarrheal deaths each year around the world (WHO 2019). The Center for Disease Control and Prevention (CDC) has indicated that 17 waterborne pathogens (bacteria, parasites, and viruses) caused 7.15 million illnesses, 6630 deaths, and $3.33 billion in direct healthcare costs in 2014. CDC estimates that each year 1 in 44 people gets sick from waterborne diseases in the U.S. (CDC 2014). Therefore, groundwater quality management has become an essential public policy (Abdalla et al. 1992), and the U.S. Environmental Protection Agency (EPA) has established the Ground Water Rule (EPA 2002) to help prevent waterborne disease outbreaks caused by contamination of groundwater in the U.S.

Viruses are generally considered to be the most dangerous microbial pathogen in groundwater because they may have a very low infectious dose. For example, the infectious dose for rotavirus strain CJN is 1, poliovirus is 2–20, norovirus is 10–100, and echovirus type 12 is 3.3×10^2 PFU (Yezli and Otter 2011). It has been estimated that 65% of the waterborne-disease outbreaks associated with groundwater contamination are caused by enteric viruses (Benedict et al. 2017, Blackburn et al. 2004, Brunkard et al. 2011, Yates et

al. 1985). Viruses are often introduced into the subsurface through sewage and wastewater effluents, septic tanks, and landfills (Yates et al. 1985) and eventually reach groundwater sources (Fong et al. 2007, Gabrieli et al. 2009, Locas et al. 2007) where they pose a potential threat to public health. Most human viruses have limited viability in the subsurface given residence times (Regnery et al. 2017, Sidhu and Toze 2012, Sidhu et al. 2010), and aquifers are often used to "polish" drinking water through soil aquifer treatment (Elkayam et al. 2018, Fox 2020, Hermes et al. 2019, Maliva 2020, Morrison et al. 2020).

Managed aquifer recharge (MAR) is a cross-cutting technology (Sprenger et al. 2017) that can be used to enhance groundwater recharge. It can be accomplished through a variety of approaches such as infiltration basins or trenches (Błażejewski et al. 2018, Chahar et al. 2012, Heilweil and Watt 2011), aquifer storage, transfer, and recovery (ASTR) (Antoniou et al. 2017, Dillon et al. 1999, Pavelic et al. 2004), flooding land (Flood-MAR) (Alam et al. 2020, Chinnasamy et al. 2018, Scherberg et al. 2014), flooding agricultural land (Ag-MAR) (Dahlke et al. 2018, Ghasemizade et al. 2019, Niswonger et al. 2017), and vadose zone recharge techniques like drywells or vadose zone pits/trench/small diameter well (Edwards 2017, Händel et al. 2014, Liang et al. 2018, Qi et al. 2020, Sasidharan et al. 2020). Various water sources are used in MAR, including snowmelt, streamflow, stormwater, recycled wastewater, excess irrigation water in agricultural fields, winter floodwater, groundwater, and reclaimed water (NGWA 2014, NRC 2008). Vadose zone recharge wells have been used successfully for many years in Scottsdale, AZ, using treated recycled water (City of Scottsdale 2020). Contamination of groundwater by stormwater drainage wells has been reported across the U.S. (Cadmus 1991, 1996, 1999, Haney et al. 1989, Michael 1997, Orr 1993, USEPA 1997, Wilde 1994). The microbial risks from MAR techniques, therefore, need to be assessed to ensure adequate protection of groundwater quality and public health.

Microbial risk assessment is an evaluation process to determine the likelihood of adverse human health effects following exposure to pathogenic microorganisms from various sources (Soller 2009). One of the commonly advocated methods for assessing microbial risks in recycled water systems is static Quantitative Microbial Risk Assessment (QMRA) (NRMMC-EPHC-AHMC 2006, Soller and Eisenberg 2008, WHO 1993). Static QMRA focuses on estimating the probability of infection to an individual due to a single exposure event (Soller and Eisenberg 2008). The QMRA approach requires quantitative input data for pathogen occurrence in the source water and their removal through treatment barriers (NRMMC-EPHC-AHMC 2006, WHO 1993). Appropriate quantification of input data and the selection of numerical values for each variable is critical for a successful risk assessment. The parameters for QMRA include the evaluation of pathogen source, concentration, an infectious dose of individual pathogen, dose-response assessment to estimate a risk of response (infection, illness, or death), human behavior (water consumption pattern and the daily intake volume), disease incidence of the local community as well as operational design and performance of the treatment barriers (Blokker et al. 2014, QMRAWiki 2014). When MAR is used as a treatment barrier and recharge option for groundwater management, the parameterization requires an understanding of pathogen transport and removal processes in the aquifer. The residence time in an aquifer has been found to play a pivotal role in allowing biological and chemical processes to improve the water quality (Dillon et al. 2003, Toze et al. 2010). The residence time for a drywell depends on the setback distance between the

drywell and a drinking water well (City of Portland 2008, City of Portland 2015, EPA 1999, Washington State Department of Ecology 2006). However, current regulatory guidelines to protect groundwater quality require an additional separation distance between the bottom of the drywell and the local groundwater table of 1.5 to 13 m (City of Portland 2008, City of Portland 2015, EPA 1999, Washington State Department of Ecology 2006).

Several field- and laboratory-scale experiments and numerical modeling approaches have been used to study virus removal and assess risk during MAR (Anders and Chrysikopoulos 2008, Jin and Flury 2002, Powelson and Gerba 1994, Stevenson et al. 2015). Toze et al. (2010) conducted an in-situ decay study at a MAR site, and 1 log reduction for rotavirus was calculated as a function of residence time to be 34 days (Toze et al. 2010). However, the MAR guideline evaluates the effectiveness of aquifer treatment (expressed as log reductions) to meet the human health-based microbial target of 1×10^{-6} DALYs (disability-adjusted life years, 6-$\log_{10}$) per person per year as a function of residence time (NRMMC-EPHC-AHMC 2006, Page et al. 2018). Current guidelines for MAR have only considered the inactivation of viruses in the liquid-phase as a reliable mechanism for virus removal but have neglected irreversible attachment and solid-phase inactivation of viruses (Abu-Ashour 1994, Dillon et al. 2008). Therefore, the QMRA approach based on liquid-phase inactivation of viruses may underestimate the virus removal during MAR operations.

Major processes controlling the transport and removal of viruses in porous media are advection, dispersion, attachment, detachment, and first-order inactivation (both liquid and solid-phase) (Schijven and Hassanizadeh 2000, Schijven et al. 2002). The rate coefficient for attachment, detachment, liquid, and solid-phase inactivation is sensitive to many physicochemical factors such as flow dynamics, porous media properties, solution chemistry, temperature, residence time, and pathogen physicochemical properties (Molnar et al. 2015, Schijven and Hassanizadeh 2000). The relative importance of these processes will determine the transport potential of viruses at MAR sites (Regnery et al. 2017, Sidhu et al. 2015, Toze et al. 2010). Therefore, several physicochemical and environmental factors may need to be optimized to ensure adequate virus removal during MAR operations. However, no previous studies have investigated a range of virus removal parameters and their impact on groundwater quality when assessing the microbial risk from a drywell operation.

The local hydrogeology and subsurface heterogeneity at a MAR site will influence the residence time, which, in turn, affects the groundwater quality. Subsurface heterogeneity, such as stratified or aggregated soils (i.e., low and high conductive soil texture), their horizontal and vertical (process such as fractures, faults, macropores, cracks, and other preferential flow paths) distribution, and connectivity, significantly impacts water flow in the subsurface (Dagan 2012, Gelhar 1986, Mantoglou and Gelhar 1987, Schilling et al. 2017, Xie et al. 2014, Yeh et al. 1985a, Yeh et al. 1985b). Our previous studies investigated the influence of stochastic subsurface heterogeneity parameters on cumulative infiltration and recharge volumes, early and late arrival times, and arrival points from a drywell under constant head conditions (Sasidharan et al. 2019, Sasidharan et al. 2020). Preferential flow paths or high permeable vertical or horizontally extended soil layers (Arnaud et al. 2015, Bradford et al. 2017) can lead to the early arrival of pathogenic microbes at the water table or nearby drinking water wells. Therefore, an understanding of the influence of

subsurface heterogeneity on virus transport during the operation of a drywell is essential when assessing water quality. However, field-scale transport experiments using pathogenic or indicator viruses poses many technical challenges in quantifying flow and transport processes, and introduced pathogens create an unacceptable risk to human health. Therefore, previous researchers have mainly conducted column scale virus experiments and inversely determined transport and fate parameters (Frohnert et al. 2014, Sasidharan et al. 2017, Schijven et al. 2002, Torkzaban et al. 2006). This information can subsequently be used in numerical experiments to investigate expected virus behavior at the field-scale (Torkzaban et al. 2019) or specific MAR sites. Nevertheless, such efforts were not made before for a drywell operation.

The objective of this study is to demonstrate the application of numerical experiments using HYDRUS (2D/3D) software coupled with column laboratory-scale data to understand the influence of subsurface heterogeneity on virus transport, where field-scale studies are not feasible. Constant head water flow simulations were conducted to obtain steady-state initial conditions in the flow domain to represent the worst-case scenario for virus transport. Additional constant head simulations for virus transport were considered in a drywell to understand the effect of various removal parameters on virus transport under homogenous and different subsurface heterogeneity conditions.

2. MATERIALS AND METHODS

2.1. Mathematical Model for Water Flow and Virus Transport

HYDRUS (2D/3D) was used to numerically solve the 2-dimensional axisymmetric form of the Richards equation with the van Genuchten (1980) and Mualem (1976) unsaturated soil hydraulic functions (Mualem 1976, van Genuchten 1980). The input parameters, initial conditions, and boundary conditions employed in these numerical experiments were generally based on results from drywells located in Fort Irwin, CA (Sasidharan et al., 2020). In brief, the water level in the Fort Irwin drywell was continuously monitored using an in-situ water level sensor and remote data acquisition techniques. The falling head phase of a filling and draining cycle in the drywell during a storm event was selected for further analysis (Sasidharan et al. 2018a, Sasidharan et al. 2020). The observed falling head data from the drywell was used in conjunction with HYDRUS (2D/3D) and the reservoir boundary condition module to inversely optimize the saturated soil hydraulic conductivity $\left(K_s = 0.046 \text{ m day}^{-1}\right)$ and the shape parameter in the soil water retention function (α=9.17 m^{-1}) (Sasidharan et al. 2018a, Šimůnek et al. 2018). The residual soil water content (θ_r=0.043), the saturated soil water content (θ_s=0.39), and the pore-size distribution parameter in the soil water retention function (n=2.76) were derived from the measured particle size distribution (silt-clay-fraction) and the Rosetta software (Schaap et al. 2001, Segal et al. 2009), whereas the tortuosity parameter in the hydraulic conductivity function (l) was set to 0.5.

Sasidharan et al. (2018b) showed in column experiments that a small fraction of the injected virus was reversibly retained and not inactivated, and the remaining fraction was irreversibly retained and inactivated on the solid phase. A one-site retention model did not account for

the reversible virus fraction and observed low concentration tailing, whereas a model with two kinetic retention sites and separate solid phase inactivation rates was needed to describe this behavior (Fig. S1). Two-site kinetic retention may occur due to spatial variability in the flow field, mass transfer, strength of adhesive, and retention mechanisms (Schijven and Simunek, 2002). In this work, the HYDRUS (2D/3D) computer code was used to simulate virus transport from a drywell under various virus removal and subsurface conditions (Šejna et al. 2014). This model solves the two-dimensional form of the advection-dispersion equation with two kinetic retention sites having different attachment and detachment coefficients and solid-phase inactivation rates. The aqueous phase and solid-phase mass balance equations for this application are given as:

$$\frac{\partial \theta C}{\partial t} = \frac{\partial}{\partial x_i}\left(\theta D_{ij}^{w}\frac{\partial C}{\partial x_j}\right) - \frac{\partial q_i C}{\partial x_i} - \theta \mu_l C - \theta k_a C + \rho_b k_{d1} S_1 + \rho_b k_{d2} S_2 \tag{1a}$$

$$\rho_b \frac{\partial S_1}{\partial t} = \theta f_r k_a C - \rho_b k_{d1} S_1 - \rho_b \mu_s S_1 \tag{1b}$$

$$\frac{\partial S_2}{\partial t} = \theta(1 - f_r) k_a C - \rho_b k_{d2} S_2 - \rho_b \mu_s S_2 \tag{1c}$$

where t [T; T denotes the dimension of time] is time, C [NL^{-3}; N denotes the virus concentration in pore-water, L denotes the dimension of length] is the aqueous phase virus concentration, ρ_b [ML^{-3}; M denotes the dimension of mass] is the bulk density, θ is the volumetric water content [−], S [NM^{-1}] is the solid-phase virus concentration, $D_{ij}^{w}[L^2\ T^{-1};]$ is the dispersion coefficient tensor for the liquid-phase (longitudinal dispersivity, D_L=6 m and transverse dispersivity, D_T=0.5 m were used), q_i [LT^{-1}] is the i-th component of the Darcian fluid flux density, x_i [L] (i=1, 2) are the spatial coordinates, k_a [T^{-1}] is the total virus attachment rate coefficient, μ_l [T^{-1}] is the liquid-phase virus inactivation rate, μ_s [T^{-1}] is the solid-phase virus inactivation rate, k_d [T^{-1}] is the virus detachment rate coefficient, and subscripts 1 and 2 on parameters indicate the solid-phase sites.

In this study, virus attachment to and detachment from the solid surface were modeled as first-order processes. The value of k_a was divided between the kinetic attachment sites using the reversible fraction, f_r, in Eqs. 1b and 1c (Bradford et al. 2016). Reversible attachment ($f_r k_a$) occurs on site 1 because $k_{d1} = 10^{-5}$ min^{-1}, whereas irreversible attachment, $(1 - f_r)k_a$, occurs on site 2 when $k_{d2} = 0$ min^{-1}. The same value of μ_s was assumed for both sites 1 and 2. According to filtration theory, the value of k_a is related to the average flow velocity as (Yao et al. 1971):

$$k_a = \frac{3}{2}\frac{(1-n)}{d_c}\alpha \eta v \tag{2}$$

where n is the porosity, d_c [L] is the median grain diameter, v [LT^{-1}] is the average pore-water velocity, η [−] is the single-collector contact efficiency representing the ratio of the number of virus approaching the collector to the number of virus striking a collector (Tufenkji and Elimelech 2004), α [−] is the sticking efficiency representing the ratio of the rate of virus that sticks to a collector to the rate at which they strike the collector. In this study, the correlation equation developed by Messina et al. (2015) was used to predict η as a function of parameters such as Peclet number and virus size (50 nm). The value of d_c in Eq. [2] was determined from the saturated hydraulic conductivity (K_s) using the Kozeny–Carman equation (Bear 1972) as follows:

$$d_c = U_i\left(\frac{K_s\mu}{\rho_w g}\frac{180(1-n)^2}{n^3}\right)^{0.5} \quad (3)$$

where $\rho_w\left[\mathrm{M\,L^{-3}}\right]$ is the density of water, $\mu\left[\mathrm{M\,L^{-1}\,T^{-1}}\right]$ is the dynamic viscosity of water, $g\left[\mathrm{L\,T^{-2}}\right]$ is the acceleration due to gravity, and U_i is the uniformity coefficient that was taken to be 4.

2.2. Numerical Experiments

A constant head recharge simulation was conducted for 365 days to achieve steady-state flow conditions (Sasidharan et al., 2020). The flow domain and water flow boundary conditions are shown in Fig. 1. Boundaries shown in blue were assigned a no-flow boundary condition (BC), drywell's screened boundaries shown in red are constant head BCs that increase in a linear manner with depth, and the green bottom boundary was a free drainage BC. Note that the free drainage condition assumes that the water table is deeper than 60 m, such that the capillary fringe does not impact the simulation results. The initial condition (IC) was specified in terms of the soil water pressure head $h(x, z)$. In this study, the final pressure head from a recharge simulation (in which the initial condition was set as a constant pressure head of −0.5m for the entire flow domain (Sasidharan et al. 2020) was imported into HYDRUS (2D/3D) and employed as the initial condition (e.g., Fig. S2). The steady-state flow field (i.e., calculate water contents and fluxes) for the virus transport simulations was determined from this IC.

The flow domain was discretized using a two-dimensional triangular finite element mesh with the MESHGEN tool available within HYDRUS (2D/3D) (Šejna et al. 2014). The mesh was refined such that the size of elements was smaller (0.05–0.25 m) near the drywell (where infiltration is simulated), and the grid size was gradually increased with radial distance from the drywell, with a maximum element size of 0.5–0.75 m. The quality of the finite element mesh was assessed by ensuring the value of mass balance error reported by HYDRUS (2D/3D) at the end of simulation was always below 1% for water flow and 2–3% for solute transport (Brunetti et al. 2017). The unit of time in the simulations was set in minute and the initial time step was 0.001 min. The minimum and maximum time steps were set at 0.0001 min and 1 min, respectively. The maximum number of iterations was set at 10, the water content tolerance was set at 0.0001 [-], and pressure head tolerance was set at 0.01 [m].

The solute transport boundary conditions are also shown in Fig. 1. In brief, a no-flux virus transport boundary condition was assigned to the upper boundary. The nodes representing the right and lower left sides of the flow domain were set to no flux boundaries. The nodes at $z = -8.7$ to -38 m (drywell sidewall) and the bottom boundary (z=−60 m) were assigned a third-type (Cauchy, mixed, or solute flux) boundary condition since the solute flux along a boundary is specified. This type of boundary condition is mass conservative. When the water flux is zero or directed out of the region, third-type boundary conditions are automatically switched to second type (Neumann) boundary conditions (Šimunek et al. 2012). The initial concentration of viruses at the flow domain was set as zero, the initial input concentration of injection water from drywell (C_0) was set as 1, and the breakthrough curve (BTC) at a specified location on the flow domain was determined as C/C_0.

Numerical experiments were conducted using HYDRUS (2D/3D) to determine the appropriate groundwater separation distance for the safe operation of a drywell to minimize groundwater contamination at the water table from a virus that is 50 nm in size. Steady-state water flow occurred in the simulation domain (a conservative flow scenario), while a 90-day step pulse of viruses was added to the drywell followed by 275-days of virus-free water. Virus BTCs were determined at depths of 1, 4, 6, 13, and 22 m below the bottom of the drywell (corresponding nodes at the left boundary of the flow domain were selected to represent a monitoring well located next to the drywell, Fig. 1). A range of virus removal parameters was selected to optimize virus transport during the drywell operation. Tables 1 and 2 show a summary of virus transport and fate parameter combinations employed in all simulations. The parameter ranges were selected to encompass reported values in the literature (Blanc and Nasser 1996, Bradford et al. 2016, Schijven and Hassanizadeh 2000, Yahya et al. 1993), and justification for inclusion or non-inclusion of different transport processes are explained in section S1.1 of the Supporting Information. Fig. 2 illustrates various virus removal processes in porous media considered in this study.

2.2.1 Homogeneous Domain—Set I and II simulations (Table 1) were conducted assuming a homogeneous domain, and hydraulic parameters were measured for the Fort Irwin, CA soil, as described in Section 2.1. Set IA simulations investigated the effect of low values of irreversible attachment by varying α from 0 to 1×10^{-3}. Additional simulations (Set IB, Table 1) were conducted to demonstrate the benefit of in-situ iron oxide treatment near the drywell on virus removal using higher values of α=0.03 and 0.47 (Ryan et al. 1999).

Set II simulations were conducted to illustrate expected virus transport and removal when $\alpha=1\times10^{-4}$ and other fate parameters were considered. Seven scenarios were considered and are referred to as the *irreversible attachment* $[(f_r = 0) + \alpha]$, *detachment* $[(f_r = 1) + \alpha + k_{d1}]$, *liquid inactivation* $[(f_r = 1) + \alpha + k_{d1} + \mu_l]$, *solid-phase inactivation* $[(f_r = 1) + \alpha + k_{d1} + \mu_l + \mu_S)]$, *reversible fraction* $[(f_r = 0.1) + \alpha + k_{d1}]$, $reversible\ fraction\ + \mu_l[(f_r = 0.1) + \alpha + k_{d1} + \mu_l]$, and $reversible\ fraction\ + \mu_l + \mu_s[(f_r = 0.1) + \alpha + k_{d1} + \mu_l + \mu_s]$ scenarios (Table 1).

2.2.2. Heterogeneous Domain—Additional numerical experiments were conducted to investigate the influence of subsurface heterogeneity on virus fate from a drywell.

Natural geological processes produce high permeable horizontal lenses and layers in soil texture and preferential water flow pathways in the vertical direction (cracks, micropores, faults, and other preferential flow paths). The HYDRUS (2D/3D) computer software has an option to generate stochastic distributions of hydraulic conductivity (α_K) and pressure head (α_h) scaling factors using the Miller-Miller similitude approximation (Miller and Miller 1956). The detailed methodology that was used to produce stochastic domains in HYDRUS (2D/3D) is explained in our previous studies (Sasidharan et al. 2019, Sasidharan et al. 2020) and is only briefly discussed in section S1.2 of the supporting information.

The following hypothetical combinations of scaling factors with variable σ (σ=0.25, 0.5, 1: when X=1 m and Z=0.1 m), X (X=0.1, 1, 10 m when σ=1 and Z=0.1 m), and Z(Z=0.1, 1, 2 m when σ=1 and X=1) were used in virus transport simulations. Similar parameter ranges have been measured in the field (Freeze 1975, Sudicky and MacQuarrie 1989) and employed in published modeling studies for other applications (Sasidharan et al. 2019, Sasidharan et al. 2020). Set III simulations (Table 1) considered the *detachment* scenario for all seven stochastic domains. Set IV simulation (Table 1) only considered the *detachment* and *reversible fraction* + μ_s + μ_l scenarios for stochastic domains X=1, Z=2, σ=1 and X=10, Z=0.1, σ=1 under steady-state flow conditions. Additional drywell simulations were conducted to demonstrate the application and upscaling of virus parameters obtained from a laboratory-scale column to field-scale studies. Set VA simulations (Table 2) were conducted using virus removal parameters taken from saturated sand-packed column experiments using bacteriophage PRD1 at 20°C (Sasidharan et al., 2018b). Set VB simulations (Table 2) were conducted using field-scale PRD1 removal parameters from a dune recharge site in the Netherlands (Schijven et al., 1999).

3. RESULT AND DISCUSSIONS

3.1. Homogeneous Soil Profiles

3.1.1. Set I - Irreversible Attachment: Numerical experiments were conducted to better understand the transport behavior of a virus from a drywell under steady-state water flow conditions. Virus removal in soils has been reported to be controlled by attachment (Sasidharan et al., 2018b). Set IA simulations (*irreversible attachment scenario*) were therefore conducted to investigate the effect of low levels of α. Low values of α were employed in these simulations to provide a best-case (greatest) virus transport scenario to assess the potential risk to human health.

Figs. 3A and 3B show the virus concentration (log scale) in the flow domain after 90 and 365 days, respectively, of steady-state water flow when $f_r = 0, k_{d1} = \mu_l = \mu_s = 0\ \text{min}^{-1}$, and α=0, 1×10^{-5}, 1×10^{-4}, and 1×10^{-3}. Note that readers could refer to Fig. S3 that explains various terms used in a representative BTC graph to interpret data easily for all the BTCs presented in this manuscript. Recall that the drywell contained virus for 90 days, and then virus-free water for another 275 days. The highest virus concentration (red) reached the bottom boundary during the 90-day pulse injection when α=0. However, the virus distribution around the drywell rapidly decreased with an increase in α and with the elution time (comparison of Figs. 3A and 3B) due to irreversible attachment. Note that the virus

concentration in the domain pore-water was almost completely eliminated after 365 days when $\alpha=1\times10^{-3}$.

Fig. 4 shows the corresponding virus breakthrough curves (BTC) (C/C_0) on a log-scale at depths of 1, 4, 6, 13, and 22 m below the bottom of the drywell. The virus concentration was higher than 6-$\log_{10}$ removal at 22 m after 90 days when $\alpha=0$, 1×10^{-5}, and 1×10^{-4}. In comparison, the virus concentration was less than 6-$\log_{10}$ at 6 m when $\alpha=1\times10^{-3}$. However, the virus concentration declined to less than 6-$\log_{10}$ after 365 days when $\alpha=1\times10^{-5}$, 1×10^{-4}, and 1×10^{-3}. The time for this observed decline at 4 m after 90 days pulse varies from 214, 15, and 1 day for $\alpha=1\times10^{-5}$, 1×10^{-4}, and 1×10^{-3}, respectively. Prolonged concentration tailing was observed in BTCs even though detachment was not considered. This tailing behavior was more pronounced when the value of α was smaller. This occurs because of physical nonequilibrium from the velocity distribution in the flow domain (Fig. S4A). In addition, k_a (Eq. 2) is also a function of the flow velocity (Johnson et al. 2007, Shen et al. 2010, Syngouna and Chrysikopoulos 2013, Syngouna et al. 2017, Torkzaban et al. 2007).

The treatment of soil material with metal oxides such as zero-valent iron, goethite, manganese oxide, and iron hydroxide has been found to greatly enhance the removal of microbial pathogens (Ahammed and Meera 2010, Kim et al. 2008, Li et al. 2014). Therefore, Set IB simulations were conducted to assess the potential benefit of iron oxide coating of soil adjacent to a drywell on virus removal. Reported values of α=0.03 and 0.47 for virus removal on iron oxide coated sand were employed for this purpose (Ryan et al., 1999). A 6-$\log_{10}$ virus removal was obtained around the drywell within <1.5 m and 0.43 m in the horizontal and vertical direction, respectively, when α=0.47 (Fig. S5A), and within <1.9 m and 0.43 m when α=0.03 (Fig. S5B). These distances are much smaller than those shown in other simulation scenarios in this paper. These results suggest that incorporating ex-situ treatment and/or in-situ treatment zones into drywell designs may be needed to ensure that recharge water from a drywell is of acceptable microbial quality. Additional research is warranted to address this issue.

3.1.2. Set II - Reversible Attachment: Virus removal in the soil below a drywell depends on other parameters besides α. Set II simulations were conducted to illustrate the expected transport and removal behavior when $\alpha=1\times10^{-4}$ and other virus fate parameters (f_r, k_{d1}, μ_l, and μ_s) were varied. Figs. 5A–5F shows the virus BTCs on a log-scale at depths of 1, 4, 6, 13, and 22 m below the bottom of the drywell when considering *detachment*, *liquid inactivation*, *solid-phase inactivation*, *reversible fraction*, *reversible fraction* + μ_l, and *reversible fraction* + μ_l + μ_s scenarios, respectively. Figs. S6A-S6F show the corresponding virus concentration (log scale) in the flow domain after 90 and 365 days, respectively.

Note that all Set II simulations were nearly identical to the *irreversible attachment* scenario (Fig. S6A) for the first 90 days of virus injection. In this case, results were controlled by the same value of $\alpha=1\times10^{-4}$. In contrast, pronounced differences occur after virus injection stopped, and elution continued (>90 days). Low levels of virus concentration tailing can occur during this time interval as a result of slow detachment ($k_{d1}=1\times10^{-5}$ m

min^{-1}) and subsequent migration of viruses. Note that nonequilibrium viral mass transfer plays a larger role in concentration tailing (Fig. 5A) than physical nonequilibrium (Fig. 4C) when $\alpha=1\times10^{-4}$. The concentration tailing level and slope depend on the presence of liquid- and solid-phase inactivation and the fraction of reversible sites. In general, liquid (Fig. 5B) and especially solid-phase (Fig. 5C) inactivation reduce the level and slope of concentration tailing in comparison to no inactivation (Fig. 5A). Higher levels and less steep slopes of concentration tailing also occur for larger reversible fractions (Fig. 5A, 5B, 5C in comparison to Figs. 5D, 5E, and 5F, respectively). The relative importance of concentration tailing also changes with depth. The peak concentration of the BTC (<90 days) is greater than the level of concentration tailing at lower depths (>90 days). In contrast, the peak concentration of the BTC can sometimes be lower than the level of concentration tailing at greater depths (e.g., Fig. 5A). This occurs because the level of concentration tailing is relatively stable with depth, whereas the peak BTC concentration strongly decreases with increasing depth due to attachment (Fig. 4).

3.2. Heterogeneous Soil Profiles

3.2.1. Set III - Detachment Scenario: Additional numerical experiments were conducted to better understand the influence of stochastic heterogeneity (X=0.1, 1, 10, Z=0.1, 1, 2, and σ=0.25, 0.5, 1) on virus transport during drywell operation. Steady-state water flow occurred during these simulations by importing the initial pressure head (Fig. S7). Fig. 6 shows the virus concentration distribution (log scale) after 365-days for Set III (*detachment scenario*) simulations. Increasing the X-correlation length (Figs. 6A, 6B, and 6C) produces a wider distribution (in the lateral direction), whereas increasing the Z-correlation length (Figs. 6D and 6E) creates a greater vertical distribution of the virus. Fig. S8 shows the virus BTC (log scale) at 3 m and 22 m for all the stochastic parameter combinations. Parameters X=1, Z=2, σ=1 produced the earliest arrival time and highest concentration at a depth of 22 m, whereas parameters X=10, Z=0.1, σ=1 resulted in the latest arrival time and lowest concentration among the stochastic parameter combinations (Fig. S8). Sasidharan et al. (2020) demonstrated that the arrival time of recharge water at the water table highly depends on the stochastic heterogeneity. For example, the arrival time was 34 days in the X=1, Z=2, σ=1 domain, 66 days in the X=10, Z=0.1, σ=1 domain, and 100 days in the X=1, Z=0.1, σ=0.25 domain. The presence of highly permeable vertical lenses facilitates the faster downward movement of water. In contrast, the domain with high permeable horizontal lenses has increased water spreading in the lateral direction. A small value of σ leads to a more uniform and lower permeability in the domain, which takes longer to fill before the wetting front arrives at the bottom boundary. Besides, the velocity distribution is also a function of stochastic parameters that lead to the physical nonequilibrium transport of viruses (Figs. S4B and S4C). Therefore, Figs. 6 and S8 confirm that the vertical flow path facilitates virus transport. In contrast, horizontally extended high permeable layers will initially promote the lateral distribution and removal of viruses before the viruses arrive at the water table, even when a low detachment rate is present.

3.2.2. Set IV - Best-case and Worst-case Scenario: Set IV simulations only considered stochastic domains X=1, Z=2, σ=1 and X=10, Z=0.1, σ=1 under the worst-case

(*detachment*) and best-case (*reversible fraction* + μ_s + μ_l) removal scenarios. Figs. 7A & 7C and Figs. 8A & 8C show the virus concentration distribution in the X=1, Z=2, σ=1 and X=10, Z=0.1, σ=1 domains, respectively, after 365 days. Similarly, Figs. 7B & 7D and Figs. 8B & 8D show the corresponding virus BTC at depths of 1, 4, 6, 13, and 22 m of the X=1, Z=2, σ=1 and X=10, Z=0.1, σ=1 domains, respectively. The virus concentration was above 6-$\log_{10,}$ even at a depth of 22 m in both domains in the worst-case (*detachment*) removal scenario. The tail concentration increased due to slow detachment and subsequent migration of viruses. In comparison to Fig. 8B (X=10, Z=0.1, σ=1), the X=1, Z=2, σ=1 domain (Fig. 7B) produced rapidly increasing concentration tailing in the deep vadose zone (13 and 22 m) due to the presence of higher velocities from permeable vertical lenses. For the best-case (*reversible fraction* + μ_s + μ_l) scenario, the 6-$\log_{10}$ removal was achieved at a depth of 22 m of the X=10, Z=0.1, σ=1 domain over 365 days. Figs. 7D and 8D show that the time required to achieve 6-$\log_{10}$ removal after 90 days pulse at a depth of 13 m was 185 days and 105 days for the X=1, Z=2, σ=1, and for X=10, Z=0.1, σ=1 flow domains, respectively.

Fig. 9 shows virus BTCs for the worst-case (Figs. 9A and 9B) and best-case (Figs. 9C and 9D) removal scenarios at a depth of 22 m of the homogeneous and heterogeneous (X=1, Z=2, σ=1, and X=10, Z=0.1, σ=1) domains. Fig. 9A shows that the virus concentration remained <6-$\log_{10}$ for the X=10, Z=0.1, σ=1 domain during the first 30 days of simulation, whereas the concentration rapidly increased >6-$\log_{10}$ after 30 days (Fig. 9B). Similarly, the virus concentration remained <6-$\log_{10}$ in both homogeneous and X=10, Z=0.1, σ=1 domains (Fig. 9C). However, the concentration was >6-$\log_{10}$ during the 15–90 day injection period and declined rapidly in the homogeneous domain, but the concentration always stayed <6-$\log_{10}$ in the X=10, Z=0.1, σ=1 stochastic domain.

3.2.3. Set V - Real-case scenarios: Sections 3.1 and 3.2 demonstrated the importance of site-specific subsurface heterogeneity and virus removal parameters in microbial risk assessment. Parameters employed in those simulations purposely represent worst-case removal scenarios to show the maximum microbial risk potential associated with drywell operation. Set VA simulations were conducted using experimentally measured viral removal parameters to evaluate several real-case scenarios using measured model parameters from field-scale (Schijven et al., 1999) or column-scale (Sasidharan et al. 2018b) studies. Table 2 provides a summary of PRD1 removal parameters from these studies used in Set VA simulations and the separation distance required to achieve a 6-$\log_{10}$ removal. A 6-$\log_{10}$ removal of PRD1 could be achieved within 1.8 m using column parameters (Sasidharan et al., 2018), whereas 7.9 m was needed when using field-scale parameters (Schijven et al., 1999). The difference in the travel distance for the PRD1 virus based on both column-scale and field-scale experiments can be explained by values of α. These observations suggest that site-specific measurements of virus transport and fate parameters ought to be employed to improve estimates of separation distance and microbial risk. For example, site-specific virus removal parameters could be determined in small-scale column studies, and then employed in field-scale modeling studies that account for site-specific hydraulic properties and subsurface heterogeneity. This approach would eliminate the need for tedious, costly, and time-consuming experimental determination of virus transport and fate in the field.

Note that virus concentrations for all the presented simulations in this study were collected from a single location at the specified depth (Fig.1) to represent the monitoring well next to the drywell, which is the current common field scale practice (worst-case scenario). In comparison, Fig. S9 compares BTCs for virus collected from a single point location (one monitoring well) with integrated values through the entire free-drainage boundary at 22 m below drywell. The integrated BTC concentration was always lower than the point location. Consequently, the BTC for a point located close to the drywell will better predict the risk associated with an early arrival time than an integrated BTC. Even though collecting an integrated BTCs for the cone of infiltration of a drywell at a field site is not practical, this study points out the benefit of installing and sampling multiple monitoring wells around the cone of infiltration (Fig. S9). Such field scale practice will help determine site-specific groundwater microbial quality, set back distance to drinking water wells, and minimize under and overestimation of the risk from a drywell.

4. FUTURE IMPLICATIONS ON REGULATORY STANDARD

Current regulatory standards for drywells only require 1.5 to 13 m separation distance between the bottom of the drywell and the local groundwater table for various cities across the U.S. (City of Portland 2008, City of Portland 2015, EPA 1999, Washington State Department of Ecology 2006). The results from Figs. 4–9, S6, S8, S9, and S10 clearly demonstrate that these regulatory standards may sometimes be inadequate to achieve a 6-$\log_{10}$ removal of viruses even at a depth of 22 m below the bottom of a drywell. The virus concentration was highly dependent on α during virus injections (<90 days) but was then controlled by small rates of detachment. Previous researchers have assumed that the threat from virus detachment was minimal (Schijven et al. 1999). However, this study showed that small α and k_d values can lead to prolonged migration and release of viruses that can adversely impact groundwater quality even for a deep water table. The threat of virus transport will be mitigated for larger α, smaller reversible fractions and detachment rates, and higher solid and liquid inactivation rates. Additional research is warranted to better understand and quantify these site-specific parameters that contribute to long-term concentration tailing. This information could be used in MAR guidelines and engineering approaches to minimize microbial contamination of groundwater.

Figs. 7 and 8 confirm that the separation distance to achieve 6-$\log_{10}$ virus removal is a function of both virus removal parameters and stochastic subsurface heterogeneity at a specific site. The presence of a vertically extended lens facilitates the rapid transport of viruses and result in an early arrival at the groundwater table. In contrast, horizontally extended lenses increase the lateral spreading and the travel time, enhancing virus removal by irreversible attachment and solid-phase inactivation, and limited vertical migration. Therefore, these factors should be considered in microbial risk assessment and separation distance requirements. The generalized use of a constant separation distance may overestimate virus removal via vadose zone treatment and potentially lead to groundwater contamination.

Fig. 9 indicates that the general assumption of a 1.5–12 m separation distance may not be adequate in some instances, and the timing of the water quality monitoring can significantly

underestimate the potential future groundwater viral contamination. These observations are consistent with reported waterborne disease outbreaks in highly heterogeneous (e.g., fractured and Karst) subsurface environments (Borchardt et al. 2011, Wallender et al. 2014), predictions of contaminant transport in stochastic systems (Mantoglou and Gelhar 1987, Yeh et al. 1985a, Yeh et al. 1985b), and simulated variations in recharge arrival times and locations below a drywell (Sasidharan et al., 2020). However, we acknowledge that the microbial risk from recharged groundwater to public health depends on various factors such as the exposure pathways, volume of injection and microbial concentration, frequency of exposure, the infectivity of the pathogen, setback distance to the drinking water well, removal within the treatment train framework, and post-treatment of recovered water. In contrast, this study explicitly points out the potential for groundwater contamination when vadose zone treatment is considered as the primary treatment barrier during MAR operation.

5. CONCLUSIONS

Numerical modeling was used to study virus transport from a drywell and the potential risk of groundwater contamination under various virus removal and subsurface heterogeneity scenarios. The separation distance between the bottom of the drywell and the bottom of the flow domain to achieve a 6-$\log_{10}$ removal of the virus was typically much larger than the currently recommended guideline of 1.5 to 13 m. Higher risks of groundwater contamination from prolonged virus concentration tailing in the deep vadose zone occurred for lower values of the sticking efficiency and liquid and solid-phase inactivation rates, and higher detachment rates and reversible fractions. Conversely, the risk from viruses can be minimized by increasing the sticking efficiency, solid-phase inactivation, and irreversible fraction of the soil around the drywell. For example, in-situ treatment with iron oxide with high sticking efficiency was found to create 6-$\log_{10}$ virus removal within 1.9 m from the drywell.

Sasidharan et al. (2017a, 2018b) demonstrated that up to 4.6 log removal of virus could be achieved by increasing the storage or residence time in a column experiment at 20ºC. Therefore, virus risk is also expected to be minimized by transient drywell operation that increases the residence time for irreversible attachment and solid-phase inactivation. Virus transport under transient conditions also involves additional processes under unsaturated conditions, such as retention at the air-water interface or remobilization during water imbibition. Therefore, transient water flow simulations were not considered in this study but warrants additional research. Site-specific sub-surface heterogeneity and hydraulic property will also influence virus transport. Horizontally extended lenses with high permeability enhance the lateral distribution and removal of the virus. Conversely, vertically extended high permeable lenses such as fractures and preferential flow pathways facilitate virus transport and will result in the rapid arrival of viruses at the groundwater table. This research illustrates that site-specific virus removal parameters obtained from the field- or column-scale experiments can be employed in field-scale modeling studies to assess risks from virus contamination and determine needed separation distances. This same approach and findings are expected to be applicable for other MAR systems (e.g., Ag-MAR and infiltration basins), as well as for septic tanks and leach fields, when vadose zone transport is considered as a treatment barrier.

Supplementary Material

Refer to Web version on PubMed Central for supplementary material.

ACKNOWLEDGMENT

Funding for this research was partially provided by the U.S. Environmental Protection Agency (US EPA) through an interagency agreement with the United States Department of Agriculture (EPA DW-012-92465401; ARS 60-2022-7--002), hatch funds CA-R-ENS-7274-H and CA-R-ENS-5047-RR from Dr. Jiří Šimůnek, University of California, Riverside, and USDA ARS National Program 211 from Dr. Scott A. Bradford, USDA Salinity Lab, Riverside. The authors would like to thank anonymous reviewers and Drs. Phil Berger and Mohamed Hantush for their constructive comments during the internal EPA review. The views expressed in this article are those of the authors and do not necessarily represent the views or policies of the U.S. Environmental Protection Agency. The mention of commercial products does not constitute an endorsement.

REFERENCE

Abdalla CW, Roach BA and Epp DJ (1992) Valuing environmental quality changes using averting expenditures: an application to groundwater contamination. Land Economics, 163–169.

Abu-Ashour J, Joy DM, Lee H, Whiteley HR and Zelin S, (1994) Transport of microorganisms through soil. Water, Air, and Soil Pollution 75(1–2), 141–158.

Ahammed MM and Meera V. (2010) Metal oxide/hydroxide-coated dual-media filter for simultaneous removal of bacteria and heavy metals from natural waters. Journal of Hazardous Materials 181(1–3), 788–793. [PubMed: 20566239]

Alam S, Gebremichael M, Li R, Dozier J. and Lettenmaier DP (2020) Can Managed Aquifer Recharge Mitigate the Groundwater Overdraft in California's Central Valley? Water Resources Research 56(8), e2020WR027244.

Anders R. and Chrysikopoulos CV (2008) Transport of Viruses Through Saturated and Unsaturated Columns Packed with Sand. Transport in Porous Media 76(1), 121–138.

Antoniou A, Smits F. and Stuyfzand P. (2017) Quality assessment of deep-well recharge applications in the Netherlands. Water Science and Technology: Water Supply 17(5), 1201–1211.

Arnaud E, Best A, Parker BL, Aravena R. and Dunfield K. (2015) Transport of through a Thick Vadose Zone. Journal of Environmental Quality 44(5), 1424–1434. [PubMed: 26436260]

Barwick RS, Levy DA, Craun GF, Beach MJ and Calderon RL (2000) Surveillance for waterborne-disease outbreaks--United States, 1997–1998. MMWR CDC Surveill Summ 49(4), 1–21.

Bear J. (1972) Dynamics of fluids in porous materials. Society of Petroleum Engineers: Dallas, TX, USA.

Benedict KM, Reses H, Vigar M, Roth DM, Roberts VA, Mattioli M, Cooley LA, Hilborn ED, Wade TJ and Fullerton KE (2017) Surveillance for waterborne disease outbreaks associated with drinking water—United States, 2013–2014. MMWR. Morbidity and Mortality Weekly Report 66(44), 1216. [PubMed: 29121003]

Blackburn BG, Craun GF, Yoder JS, Hill V, Calderon RL, Chen N, Lee SH, Levy DA and Beach MJ (2004) Surveillance for waterborne-disease outbreaks associated with drinking water—United States, 2001–2002. MMWR Surveill Summ 53(8), 23–45. [PubMed: 15499307]

Blanc R. and Nasser A. (1996) Effect of effluent quality and temperature on the persistence of viruse in soil. Water Science and Technology 33(10–11), 237–242.

Błażejewski R, Nieć J, Murat-Błażejewska S. and Zawadzki P. (2018) Comparison of infiltration models with regard to design of rectangular infiltration trenches. Hydrological Sciences Journal 63(11), 1707–1716.

Blokker M, Smeets P. and Medema G. (2014) QMRA in the Drinking Water Distribution System. Procedia Engineering 89, 151–159.

Borchardt MA, Bradbury KR, Alexander EC Jr., Kolberg RJ, Alexander SC, Archer JR, Braatz LA, Forest BM, Green JA and Spencer SK (2011) Norovirus outbreak caused by a new septic system in a dolomite aquifer. Ground Water 49(1), 85–97. [PubMed: 20199588]

Bradford SA, Kim H, Headd B. and Torkzaban S. (2016) Evaluating the Transport of Bacillus subtilis Spores as a Potential Surrogate for Cryptosporidium parvum Oocysts. Environmental Science & Technology 50(3), 1295–1303. [PubMed: 26720840]

Bradford SA, Leij FJ, Schijven J. and Torkzaban S. (2017) Critical Role of Preferential Flow in Field-Scale Pathogen Transport and Retention. Vadose Zone Journal 16(4).

Brunetti G, Šimůnek J, Turco M. and Piro P. (2017) On the use of surrogate-based modeling for the numerical analysis of Low Impact Development techniques. Journal of Hydrology 548, 263–277.

Brunkard JM, Ailes E, Roberts VA, Hill V, Hilborn ED, Craun GF, Rajasingham A, Kahler A, Garrison L. and Hicks L. (2011) Surveillance for waterborne disease outbreaks associated with drinking water—United States, 2007–2008. MMWR Surveill Summ 60(12), 38–68. [PubMed: 21937977]

Cadmus (1991) Storm Water Drainage Wells (5D2). Group, T.C. (ed), Waltham, MA.

Cadmus (1996) Storm Water Drainage Well Guidance - Draft. Group, T.C. (ed), Waltham, MA.

Cadmus (1999) State-by-State Notebooks Compiling Results from the Class V Underground Injection Control Study, United States Environmental Protection Agency.

CDC (2014) Waterborne Disease & Outbreak Surveillance Reporting, Centers for Disease Control and Prevention, USA.

Chahar BR, Graillot D. and Gaur S. (2012) Storm-water management through infiltration trenches. Journal of Irrigation and Drainage Engineering 138(3), 274–281.

Chinnasamy P, Muthuwatta L, Eriyagama N, Pavelic P. and Lagudu S. (2018) Modeling the potential for floodwater recharge to offset groundwater depletion: a case study from the Ramganga basin, India. Sustainable Water Resources Management 4(2), 331–344.

City of Portland O. (2008) Decision Making Framework for Groundwater Protectiveness Demonstrations, City of Portland, Bureau of Environmental Services.

City of Portland O. (2015) Underground Injection Control Management Plan, p. 53, City of Portland, Bureau of Environmental Services.

City of Scottsdale (2020) Water Supply. Scottsdale, C.o (ed), City of Scottsdale.

Dagan G. (2012) Flow and transport in porous formations, Springer Science & Business Media.

Dahlke HE, LaHue GT, Mautner MR, Murphy NP, Patterson NK, Waterhouse H, Yang F. and Foglia L. (2018) Advances In Chemical Pollution, Environmental Management and Protection, pp. 215–275, Elsevier.

Dillon P, Page D, Vanderzalm J, Pavelic P, Toze S, Bekele E, Sidhu J, Prommer H, Higginson S, Regel R, Rinck-Pfeiffer S, Purdie M, Pitman C. and Wintgens T. (2008) A critical evaluation of combined engineered and aquifer treatment systems in water recycling, pp. 753–762.

Dillon P, Toze S, Pavelic P, Ragusa S, Wright M, Peter P, Martin R, Gerges N. and Rinck-Pfeiffer S. (1999) Storing recycled water in an aquifer: Benefits and risks. Water 26(5), 21–29.

Dillon P, Toze S, Pavelic P, Skjemstad J, Davis G, Miller R, Correll R, Kookana R, Ying G. and Herczeg A. (2003) Water quality improvements during aquifer storage and recovery.

Dowd SE, Pillai SD, Wang S. and Corapcioglu MY (1998) Delineating the specific influence of virus isoelectric point and size on virus adsorption and transport through sandy soils. Applied and Environmental Microbiology 64(2), 405–410. [PubMed: 9464373]

Edwards EC (2017) Assessing the Groundwater Contamination Risk of Drywell-Induced Stormwater Infiltration Using Analytical and Numerical Methods, University of California, Davis.

Elkayam R, Aharoni A, Vaizel-Ohayon D, Sued O, Katz Y, Negev I, Marano R, Cytryn E, Shtrasler L. and Lev O. (2018) Viral and microbial pathogens, indicator microorganisms, microbial source tracking indicators, and antibiotic resistance genes in a confined managed effluent recharge system. Journal of Environmental Engineering 144(3), 05017011.

EPA (1999) The Class V Underground Injection Control Study, p. 99, United States Environmental Protection Agency, Office of Ground Water Drinking Water.

EPA (2002) National primary drinking water regulations: Long Term 1 Enhanced Surface Water Treatment Rule. Final rule, p. 1811, Environmental Protection Agency.

Feighery J, Mailloux BJ, Ferguson AS, Ahmed KM, van Geen A. and Culligan PJ (2013) Transport of E. coli in Aquifer Sediments of Bangladesh: Implications for Widespread Microbial

Contamination of Groundwater. Water Resources Research 49(7), 3897–3911. [PubMed: 24653543]

Fong TT, Mansfield LS, Wilson DL, Schwab DJ, Molloy SL and Rose JB (2007) Massive microbiological groundwater contamination associated with a waterborne outbreak in Lake Erie, South Bass Island, Ohio. Environ Health Perspect 115(6), 856–864. [PubMed: 17589591]

Fox P. (2020) Management of aquifer recharge for sustainability, pp. 21–26, CRC Press.

Freeze RA (1975) A stochastic-conceptual analysis of one-dimensional groundwater flow in nonuniform homogeneous media. Water Resources Research 11(5), 725–741.

Frohnert A, Apelt S, Klitzke S, Chorus I, Szewzyk R. and Selinka HC (2014) Transport and removal of viruses in saturated sand columns under oxic and anoxic conditions--Potential implications for groundwater protection. International Journal of Hygiene and Environmental Health 217(8), 861–870. [PubMed: 25024100]

Gabrieli R, Maccari F, Ruta A, Pana A. and Divizia M. (2009) Norovirus detection in groundwater. Food and Environmental Virology 1(2), 92–96.

Gelhar LW (1986) Stochastic subsurface hydrology from theory to applications. Water Resources Research 22(9S), 135S–145S.

Ghasemizade M, Asante KO, Petersen C, Kocis T, Dahlke HE and Harter T. (2019) An integrated approach toward sustainability via groundwater banking in the southern Central Valley, California. Water Resources Research 55(4), 2742–2759.

Gleeson T, Wada Y, Bierkens MF and van Beek LP (2012) Water balance of global aquifers revealed by groundwater footprint. Nature 488(7410), 197–200. [PubMed: 22874965]

Gunnarsdottir M, Gardarsson S. and Andradottir H. (2013) Microbial contamination in groundwater supply in a cold climate and coarse soil: case study of norovirus outbreak at Lake Mývatn, Iceland. Hydrology Research 44(6), 1114–1128.

Händel F, Liu G, Dietrich P, Liedl R. and Butler JJ Jr (2014) Numerical assessment of ASR recharge using small-diameter wells and surface basins. Journal of Hydrology 517, 54–63.

Haney J, Leach M. and Sobchak L. (1989) Dry Wells – Solution or Pollution?, Arizona Department of Environmental Quality, Phoenix, Arizona.

Heilweil VM and Watt DE (2011) Trench infiltration for managed aquifer recharge to permeable bedrock. Hydrological Processes 25(1), 141–151.

Hermes N, Jewell K, Schulz M, Müller J, Hübner U, Wick A, Drewes J. and Ternes T. (2019) Elucidation of removal processes in sequential biofiltration (SBF) and soil aquifer treatment (SAT) by analysis of a broad range of trace organic chemicals (TOrCs) and their transformation products (TPs). Water Research 163, 114857. [PubMed: 31336207]

Jin Y. and Flury M. (2002) Fate and transport of viruses in porous media. Advances in Agronomy 77, 39–102.

Johnson WP, Li X. and Assemi S. (2007) Deposition and re-entrainment dynamics of microbes and non-biological colloids during non-perturbed transport in porous media in the presence of an energy barrier to deposition. Advances in Water Resources 30(6–7), 1432–1454.

Kauppinen A, Pitkanen T. and Miettinen IT (2018) Persistent Norovirus Contamination of Groundwater Supplies in Two Waterborne Outbreaks. Food and Environmental Virology 10(1), 39–50. [PubMed: 29022247]

Keswick B.H.a.G., C.P., (1980) Viruses in groundwater. Environmental Science & Technology Letters 14(11), 1290–1297.

Kim SB, Park SJ, Lee CG, Choi NC and Kim DJ (2008) Bacteria transport through goethite-coated sand: effects of solution pH and coated sand content. Colloids and Surfaces B: Biointerfaces 63(2), 236–242. [PubMed: 18226508]

Levy DA, Bens MS, Craun GF, Calderon RL and Herwaldt BL (1998) Surveillance for waterborne-disease outbreaks--United States, 1995–1996. MMWR CDC Surveill Summ 47(5), 1–34.

Li YL, Deletic A. and McCarthy DT (2014) Removal of E. coli from urban stormwater using antimicrobial-modified filter media. Journal of Hazardous Materials 271, 73–81. [PubMed: 24607527]

Liang X, Zhan H. and Zhang YK (2018) Aquifer recharge using a vadose zone infiltration well. Water Resources Research 54(11), 8847–8863.

Locas A, Barthe C, Barbeau B, Carriere A. and Payment P. (2007) Virus occurrence in municipal groundwater sources in Quebec, Canada. Canadian Journal of Microbiology 53(6), 688–694. [PubMed: 17668028]

Maliva RG (2020) Anthropogenic Aquifer Recharge, pp. 623–645, Springer.

Mantoglou A. and Gelhar LW (1987) Effective hydraulic conductivities of transient unsaturated flow in stratified soils. Water Resources Research 23(1), 57–67.

Messina F, Marchisio DL and Sethi R. (2015) An extended and total flux normalized correlation equation for predicting single-collector efficiency. Journal of Colloid Interface Science 446, 185–193. [PubMed: 25666460]

Michael E. (1997) St. Joseph County Health Dept. Letter to Alan Melcer, US Environmental Protection Agency, Underground Control Branch, Chicago, IL, Mishawaka, IN.

Miller E. and Miller R. (1956) Physical theory for capillary flow phenomena. Journal of Applied Physics 27(4), 324–332.

Molnar IL, Johnson WP, Gerhard JI, Willson CS and O'Carroll DM (2015) Predicting colloid transport through saturated porous media: A critical review. Water Resources Research 51(9), 6804–6845.

Morrison CM, Betancourt WQ, Quintanar DR, Lopez GU, Pepper IL and Gerba CP (2020) Potential indicators of virus transport and removal during soil aquifer treatment of treated wastewater effluent. Water Research 177, 115812. [PubMed: 32311575]

Mualem Y. (1976) A new model for predicting the hydraulic conductivity of unsaturated porous media. Water Resources Research 12(3), 513–522.

NGWA (2014) Managed Aquifer Recharge, National Ground Water Association.

Niswonger RG, Morway ED, Triana E. and Huntington JL (2017) Managed aquifer recharge through off-season irrigation in agricultural regions. Water Resources Research 53(8), 6970–6992.

NRC (2008) Prospects for managed underground storage of recoverable water, National Academies Press, National Research Council.

NRMMC-EPHC-AHMC (2006) Australian guidelines for water recycling. Managing health and environmental risks. Phase 1. National Water Quality Management Strategy 21.

Orr VJ (1993) Wellhead Protection - Lessons Learned. Journal of Applied Ground Water Protection Volume 1, Number 1.

Page D, Bekele E, Vanderzalm J. and Sidhu J. (2018) Managed aquifer recharge (MAR) in sustainable urban water management. Water 10(3), 239.

Pavelic P, Dillon PJ and Robinson N. (2004) Groundwater modelling to assist well-field design and operation for the ASTR Trial at Salisbury, South Australia, Citeseer.

Pitkänen T, Karinen P, Miettinen IT, Lettojärvi H, Heikkilä A, Maunula R, Aula V, Kuronen H, Vepsäläinen A. and Nousiainen L-L (2011) Microbial contamination of groundwater at small community water supplies in Finland. Ambio: A Journal of the Human Environment 40(4), 377–390.

Powell KL, Taylor RG, Cronin AA, Barrett MH, Pedley S, Sellwood J, Trowsdale SA and Lerner DN (2003) Microbial contamination of two urban sandstone aquifers in the UK. Water Research 37(2), 339–352. [PubMed: 12502063]

Powelson DK and Gerba CP (1994) Virus removal from sewage effluents during saturated and unsaturated flow through soil columns. Water Research 28(10), 2175–2181.

Qi C, Zhan H, Liang X. and Ma C. (2020) Influence of time-dependent ground surface flux on aquifer recharge with a vadose zone injection well. Journal of Hydrology 584, 124739.

QMRAWiki (2014) Dose response assessment Center for Advancing Microbial Risk Assessment.

Regnery J, Gerba CP, Dickenson ER and Drewes JE (2017) The importance of key attenuation factors for microbial and chemical contaminants during managed aquifer recharge: a review. Critical Reviews in Environmental Science and Technology 47(15), 1409–1452.

Ryan JN, Elimelech M, Ard RA, Harvey RW and Johnson PR (1999) Bacteriophage PRD1 and Silica Colloid Transport and Recovery in an Iron Oxide-Coated Sand Aquifer. Environmental Science & Technology 33(1), 63–73.

Sasidharan S, Bradford SA, Simunek J, De Jong B. and S RK (2018a) Evaluating drywells for stormwater management and enhanced aquifer recharge. Advances in Water Resources 116, 167–177. [PubMed: 30245542]

Sasidharan S, Bradford SA, Simunek J. and Kraemer SR (2019) Drywell infiltration and hydraulic properties in heterogeneous soil profiles. Journal of Hydrology (Amst) 570, 598–611.

Sasidharan S, Bradford SA, Šimůnek J. and Kraemer SR (2020) Groundwater recharge from drywells under constant head conditions. Journal of Hydrology 583, 124569. [PubMed: 33364636]

Sasidharan S, Bradford SA, Simunek J. and Torkzaban S. (2018b) Minimizing Virus Transport in Porous Media by Optimizing Solid Phase Inactivation. Journal of Environmental Quality 47(5), 1058–1067. [PubMed: 30272798]

Sasidharan S, Bradford SA, Simunek J, Torkzaban S. and Vanderzalm J. (2017) Transport and fate of viruses in sediment and stormwater from a Managed Aquifer Recharge site. Journal of Hydrology 555(Supplement C), 724–735.

Schaap MG, Leij FJ and van Genuchten MT (2001) rosetta : a computer program for estimating soil hydraulic parameters with hierarchical pedotransfer functions. Journal of Hydrology 251(3–4), 163–176.

Scherberg J, Baker T, Selker JS and Henry R. (2014) Design of managed aquifer recharge for agricultural and ecological water supply assessed through numerical modeling. Water Resources Management 28(14), 4971–4984.

Schijven JF and Hassanizadeh SM (2000) Removal of viruses by soil passage: Overview of modeling, processes, and parameters. Critical Reviews in Environmental Science and Technology 30(1), 49–127.

Schijven JF, Hassanizadeh SM and De Bruin RHAM (2002) Two-site kinetic modeling of bacteriophages transport through columns of saturated dune sand. Journal of Contaminant Hydrology 57(3–4), 259–279. [PubMed: 12180812]

Schijven JF, Hoogenboezem W, Hassanizadeh M. and Peters JH (1999) Modeling removal of bacteriophages MS2 and PRD1 by dune recharge at Castricum, Netherlands. Water Resources Research 35(4), 1101–1111.

Schilling OS, Irvine DJ, Hendricks Franssen HJ and Brunner P. (2017) Estimating the spatial extent of unsaturated zones in heterogeneous river-aquifer systems. Water Resources Research 53(12), 10583–10602.

Segal E, Shouse PJ, Bradford SA, Skaggs TH and Corwin DL (2009) Measuring particle size distribution using laser diffraction: implications for predicting soil hydraulic properties. Soil Science 174(12), 639–645.

Šejna M, Šimůnek J. and van Genuchten MT (2014) The HYDRUS Software Package for Simulating the Two- and Three-Dimensional Movement of Water, Heat, and Multiple Solutes in Variably-Saturated Porous Media.

Shen C, Huang Y, Li B. and Jin Y. (2010) Predicting attachment efficiency of colloid deposition under unfavorable attachment conditions. Water Resources Research 46(11), n/a-n/a.

Sidhu JP, Toze S, Hodgers L, Barry K, Page D, Li Y. and Dillon P. (2015) Pathogen Decay during Managed Aquifer Recharge at Four Sites with Different Geochemical Characteristics and Recharge Water Sources. Journal of Environmental Quality 44(5), 1402–1412. [PubMed: 26436258]

Sidhu JPS and Toze S. (2012) Assessment of pathogen survival potential during managed aquifer recharge with diffusion chambers. Journal of Applied Microbiology 113(3), 693–700. [PubMed: 22702409]

Sidhu JPS, Toze S, Hodgers L, Shackelton M, Barry K, Page D. and Dillon P. (2010) Pathogen inactivation during passage of stormwater through a constructed reedbed and aquifer transfer, storage and recovery. Water Science and Technology 62(5), 1190–1197. [PubMed: 20818064]

Šimůnek J, Šejna M. and van Genuchten MT (2018) New features of version 3 of the HYDRUS (2D/3D) computer software package. Journal of Hydrology and Hydromechanics 66(2), 133–142.

Šimunek J, van Genuchten MT and Šejna M. (2012) The HYDRUS Software Package for Simulating the Two- and Three-Dimensional Movement of Water, Heat, and Multiple Solutes in Variably-Saturated Porous Media.

Soller JA (2009) The potential implications of person-to-person transmission of viral infection for US EPA's Groundwater Rule. Journal Water Health 7(2), 208–223.

Soller JA and Eisenberg JN (2008) An evaluation of parsimony for microbial risk assessment models. Environmetrics: The Official Journal Of The International Environmetrics Society 19(1), 61–78.

Sprenger C, Hartog N, Hernández M, Vilanova E, Grützmacher G, Scheibler F. and Hannappel S. (2017) Inventory of managed aquifer recharge sites in Europe: historical development, current situation and perspectives. Hydrogeology Journal 25(6), 1909–1922.

Stevenson ME, Sommer R, Lindner G, Farnleitner AH, Toze S, Kirschner AK, Blaschke AP and Sidhu JP (2015) Attachment and Detachment Behavior of Human Adenovirus and Surrogates in Fine Granular Limestone Aquifer Material. Journal of Environmental Quality 44(5), 1392–1401. [PubMed: 26436257]

Sudicky E. and MacQuarrie K. (1989) Behaviour of biodegradable organic contaminants in random stationary hydraulic conductivity fields, In Contaminant Transport in Groundwater, Proceedings of an International Symposium.(eds Kobus HE & Kinzelbach W). AA Balkema Rotterdam-Brookfield, International, Rotterdam. pp. 307–315.

Syngouna VI and Chrysikopoulos CV (2013) Cotransport of clay colloids and viruses in water saturated porous media. Colloids and Surfaces A: Physicochemical and Engineering Aspects 416, 56–65.

Syngouna VI, Chrysikopoulos CV, Kokkinos P, Tselepi MA and Vantarakis A. (2017) Cotransport of human adenoviruses with clay colloids and TiO2 nanoparticles in saturated porous media: Effect of flow velocity. Science of the Total Environment 598, 160–167. [PubMed: 28441594]

Taylor RG, Scanlon B, Döll P, Rodell M, Van Beek R, Wada Y, Longuevergne L, Leblanc M, Famiglietti JS and Edmunds M. (2013) Ground water and climate change. Nature Climate Change 3(4), 322–329.

Torkzaban S, Bradford SA and Walker SL (2007) Resolving the coupled effects of hydrodynamics and DLVO forces on colloid attachment in porous media. Langmuir 23(19), 9652–9660. [PubMed: 17705511]

Torkzaban S, Hassanizadeh SM, Schijven JF, de Bruin HAM and de Roda Husman AM (2006) Virus Transport in Saturated and Unsaturated Sand Columns. Vadose Zone Journal 5(3), 877–885.

Torkzaban S, Hocking M, Bradford SA, Tazehkand SS, Sasidharan S. and Šimůnek J. (2019) Modeling Virus Transport and Removal during Storage and Recovery in Heterogeneous Aquifers. Journal of Hydrology 578, 124082.

Toze S, Bekele E, Page D, Sidhu J. and Shackleton M. (2010) Use of static quantitative microbial risk assessment to determine pathogen risks in an unconfined carbonate aquifer used for managed aquifer recharge. Water Research 44(4), 1038–1049. [PubMed: 19762063]

Tufenkji N. and Elimelech M. (2004) Correlation equation for predicting single-collector efficiency in physicochemical filtration in saturated porous media. Environmental Science & Technology 38(2), 529–536. [PubMed: 14750730]

USEPA (1997) Superfund Web Site. Available at: http://www.epa.gov/superfund/oerr/impm/products/rodsites and http://www.epa.gov/superfund/oerr/impm/products/Cursites/cercinf.htm.

van Genuchten MT (1980) A closed-form equation for predicting the hydraulic conductivity of unsaturated soils. Soil Science Society of America Journal 44(5), 892–898.

Wallender EK, Ailes EC, Yoder JS, Roberts VA and Brunkard JM (2014) Contributing factors to disease outbreaks associated with untreated groundwater. Ground Water 52(6), 886–897. [PubMed: 24116713]

Washington State Department of Ecology (2006) Guidance for UIC Wells that Manage Stormwater, p. 58, Washington State Department of Ecology Water Quality Program.

WHO (1993) Guidelines for drinking-water quality, World Health Organization.

WHO (2019) Drinking-water, World Health Organization.

Wilde F. (1994) Geochemistry and Factors Affecting Ground Water Quality at Three Storm Water Management Sites in Maryland, US Geological Survey, [Washington, DC]

Xie Y, Cook PG, Brunner P, Irvine DJ and Simmons CT (2014) When can inverted water tables occur beneath streams? Groundwater 52(5), 769–774.

Yahya M, Cluff C. and Gerba CP (1993) Virus removal by slow sand filtration and nanofiltration. Water Science and Technology 27(3–4), 445–448.

Yao K-M, Habibian MT and O'Melia CR (1971) Water and waste water filtration. Concepts and applications. Environmental Science & Technology 5(11), 1105–1112.

Yates MV, Gerba CP and Kelley LM (1985) Virus persistence in groundwater. Applied and Environmental Microbiology 49(4), 778–781. [PubMed: 4004211]

Yeh TCJ, Gelhar LW and Gutjahr AL (1985a) Stochastic analysis of unsaturated flow in heterogeneous soils: 1. Statistically isotropic media. Water Resources Research 21(4), 447–456.

Yeh TCJ, Gelhar LW and Gutjahr AL (1985b) Stochastic Analysis of Unsaturated Flow in Heterogeneous Soils: 3. Observations and Applications. Water Resources Research 21(4), 465–471.

Yezli S. and Otter JA (2011) Minimum infective dose of the major human respiratory and enteric viruses transmitted through food and the environment. Food and Environmental Virology 3(1), 1–30. [PubMed: 35255645]

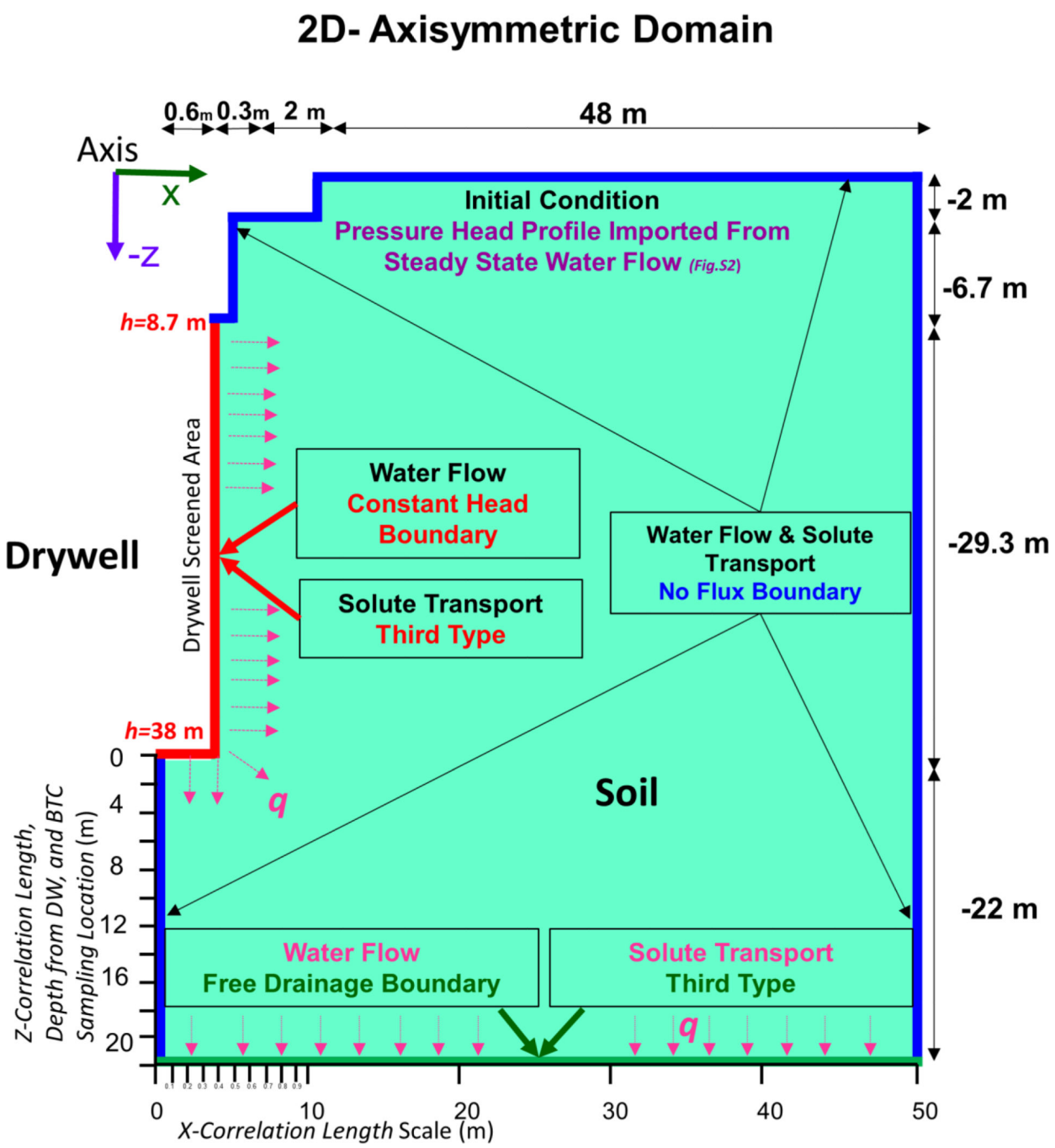

Fig. 1.

The drywell geometry, dimensions, initial condition, the boundary conditions, and the X and Z-correlation length scales (virus BTC sampling location depth corresponding to the Z-axis) for the 2D-axisymmetrical flow domain for the water flow and solute transport. The detailed drywell geometry and the water flow dynamics were presented in our previous study (Sasidharan et al., 2018a).

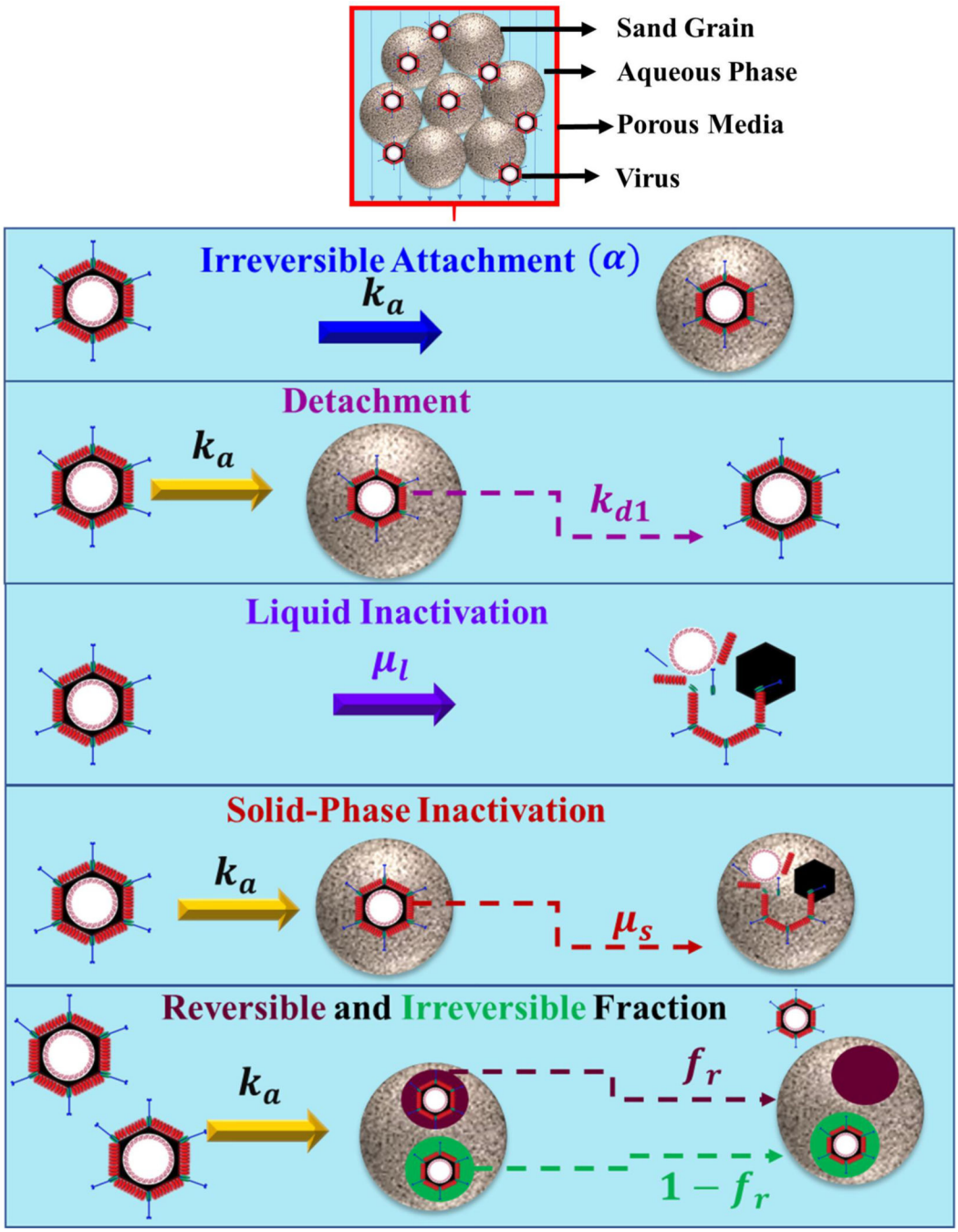

Fig. 2.

The schematic of various virus removal processes during transport in porous media that were applied in the numerical experiments presented in this study.

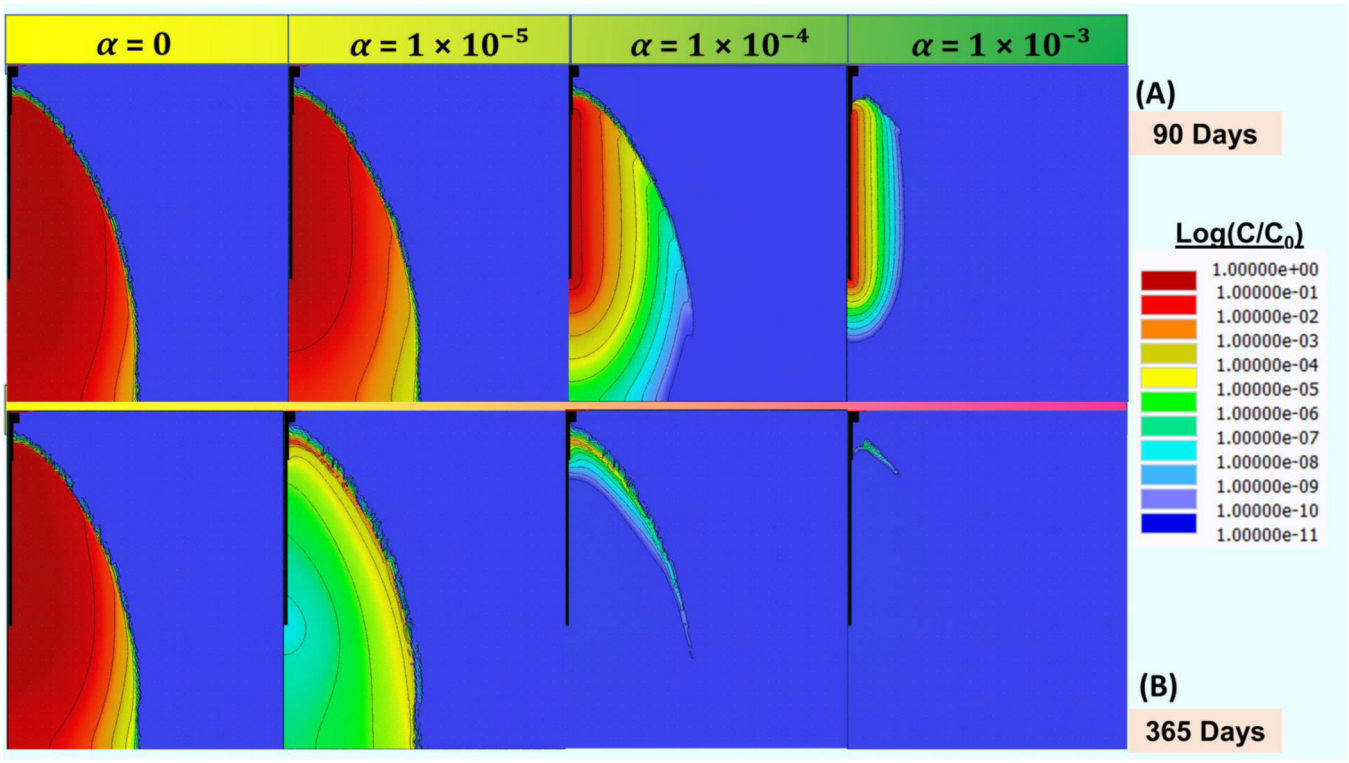

Fig. 3.

The virus removal (log scale) for the *irreversible attachment scenario* at various sticking efficiencies (α)=0, 1×10^{-5}, 1×10^{-4}, and 1×10^{-3} when detachment coefficient (k_d)=0 in a homogeneous domain (Fort Irwin Soil) after 90 days of a continuous pulse of virus **(A)** and the 365th day of steady-state virus-free water flow **(B)**.

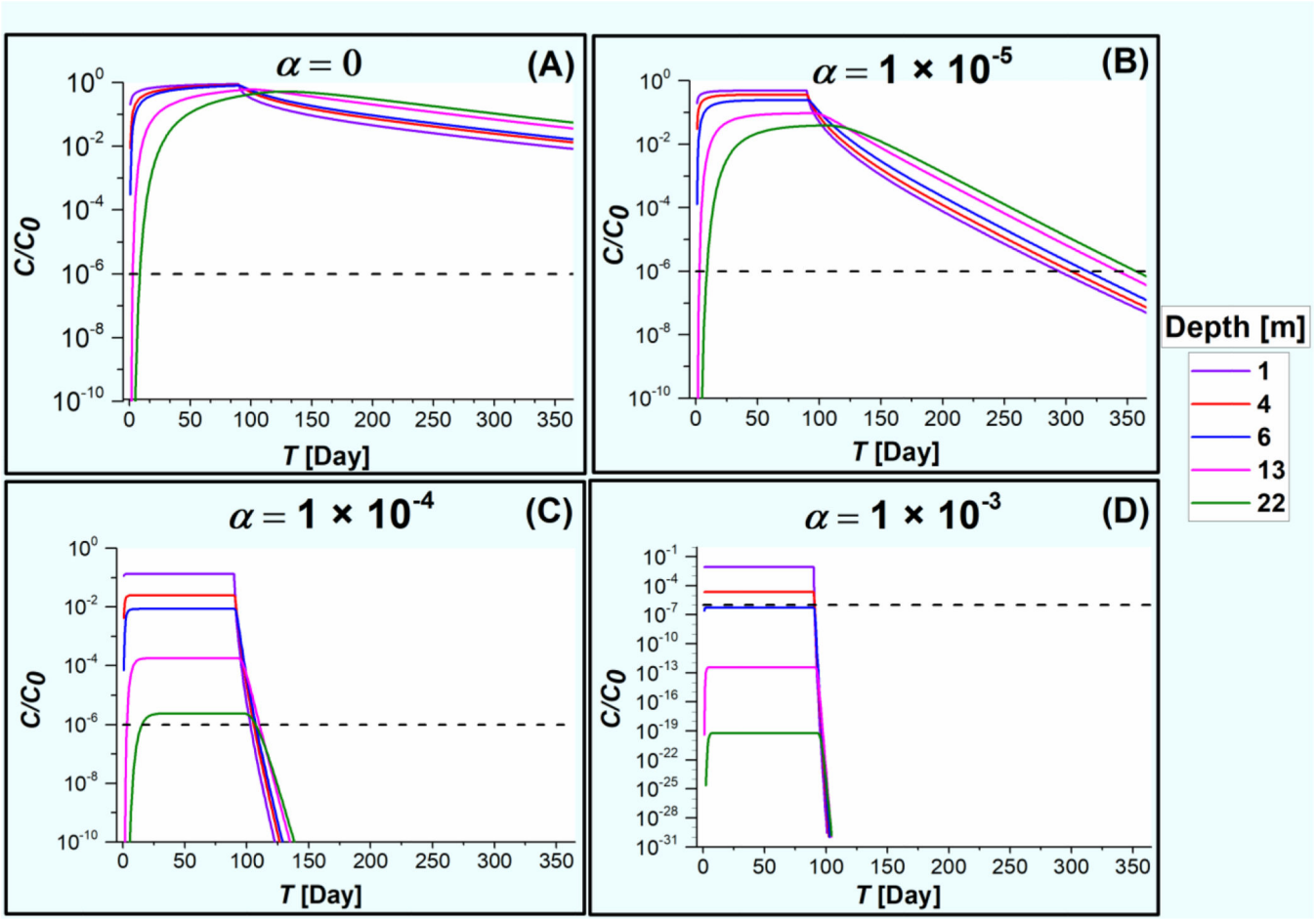

Fig. 4.

The virus breakthrough curve (log scale) for the *irreversible attachment scenario* when sticking efficiency (α)=0 **(A)**, 1×10^{-5} **(B)**, 1×10^{-4} **(C)**, and 1×10^{-3} **(D)** at depths=1, 4, 6, 13, and 22 m when the detachment coefficient (k_d)=0 in a homogeneous domain (Fort Irwin Soil) over 365 days (90 days of a continuous pulse of virus and 275-days of steady-state virus-free water flow) simulation.

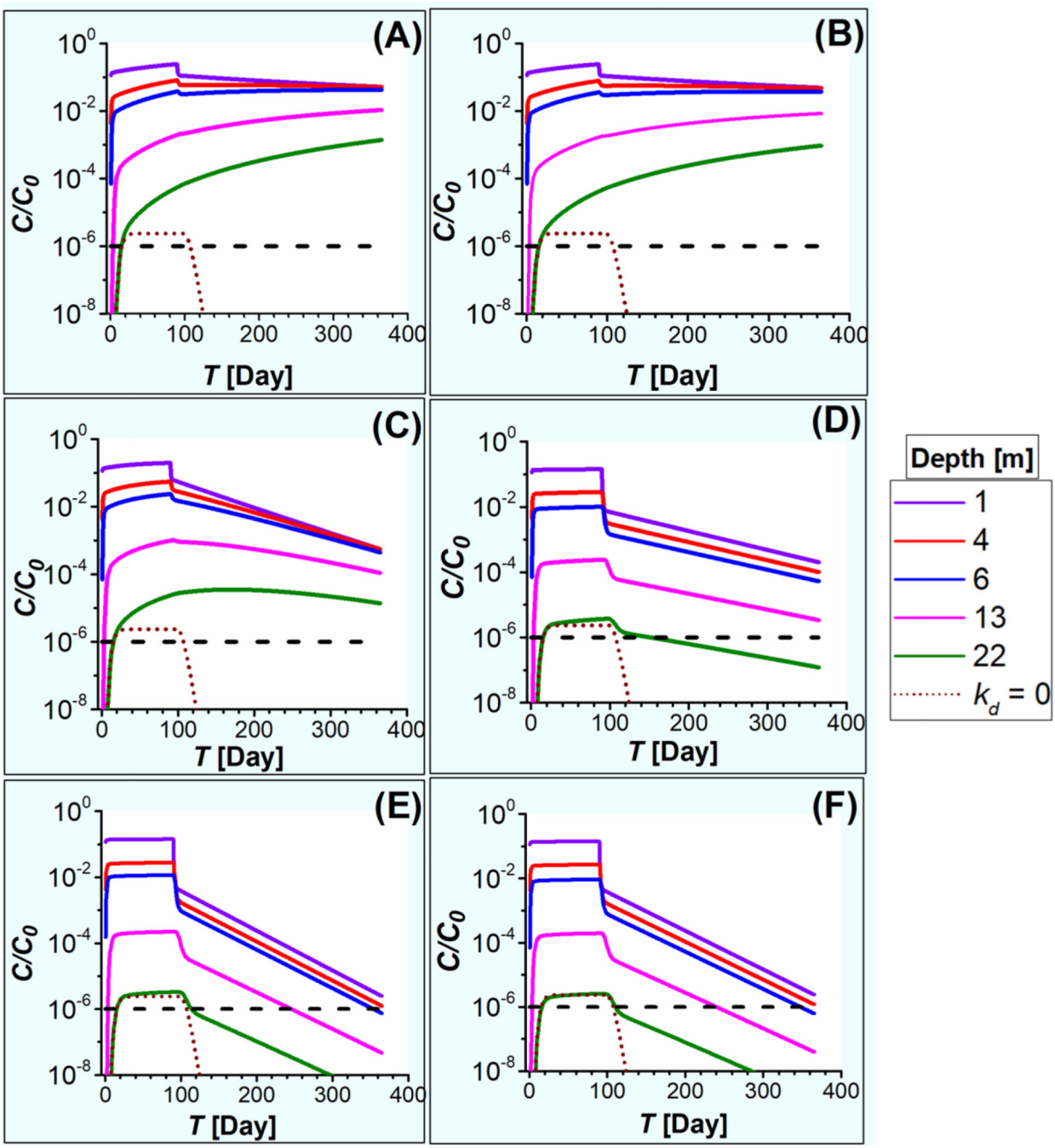

Fig. 5.

The virus breakthrough curve (log scale) at depths=1, 4, 6, 13, and 22 m for the *detachment* **(A)**, *liquid inactivation* **(B)**, *solid-phase inactivation* **(C)**, *reversible fraction* **(D)**, *reversible fraction*+μ_s **(E),** and *reversible fraction*+μ_s + μ_l **(F)** scenarios. The *Irreversible attachment scenario* is presented as the doted (brown) line. The 6-$\log_{10}$ removal is shown as the dashed blue line. Table 1 (Set I and Set II) shows the corresponding virus removal parameters.

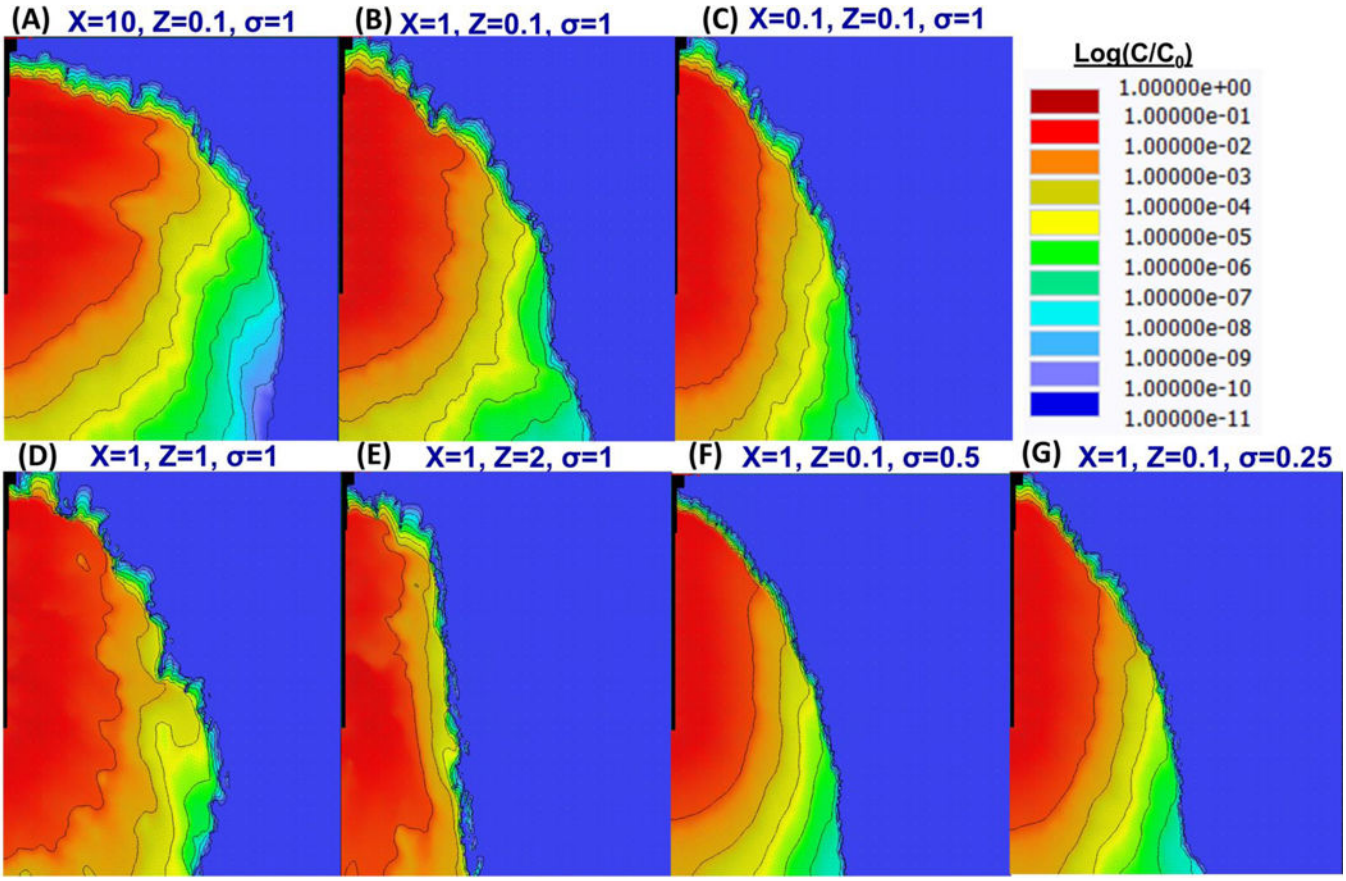

Fig. 6.

The virus concentration distribution profile (log scale) for heterogeneous X=10, Z=0.1, σ=1 (horizontal lens) **(A)**, X=1, Z=0.1, σ=1 **(B)**, X=0.1, Z=0.1, σ=1 **(C)**, X=1, Z=1, σ=1 **(D)**, X=1, Z=2, σ=1 (thick vertical lens) **(E)**, X=1, Z=0.1, σ=0.5 **(F)**, and X=1, Z=0.1, σ=0.25 **(G)**) Fort Irwin soil flow domains at 365 day after 90 days of a continuous pulse of virus transport and 275-days of steady-state water flow simulation for *detachment scenario*.

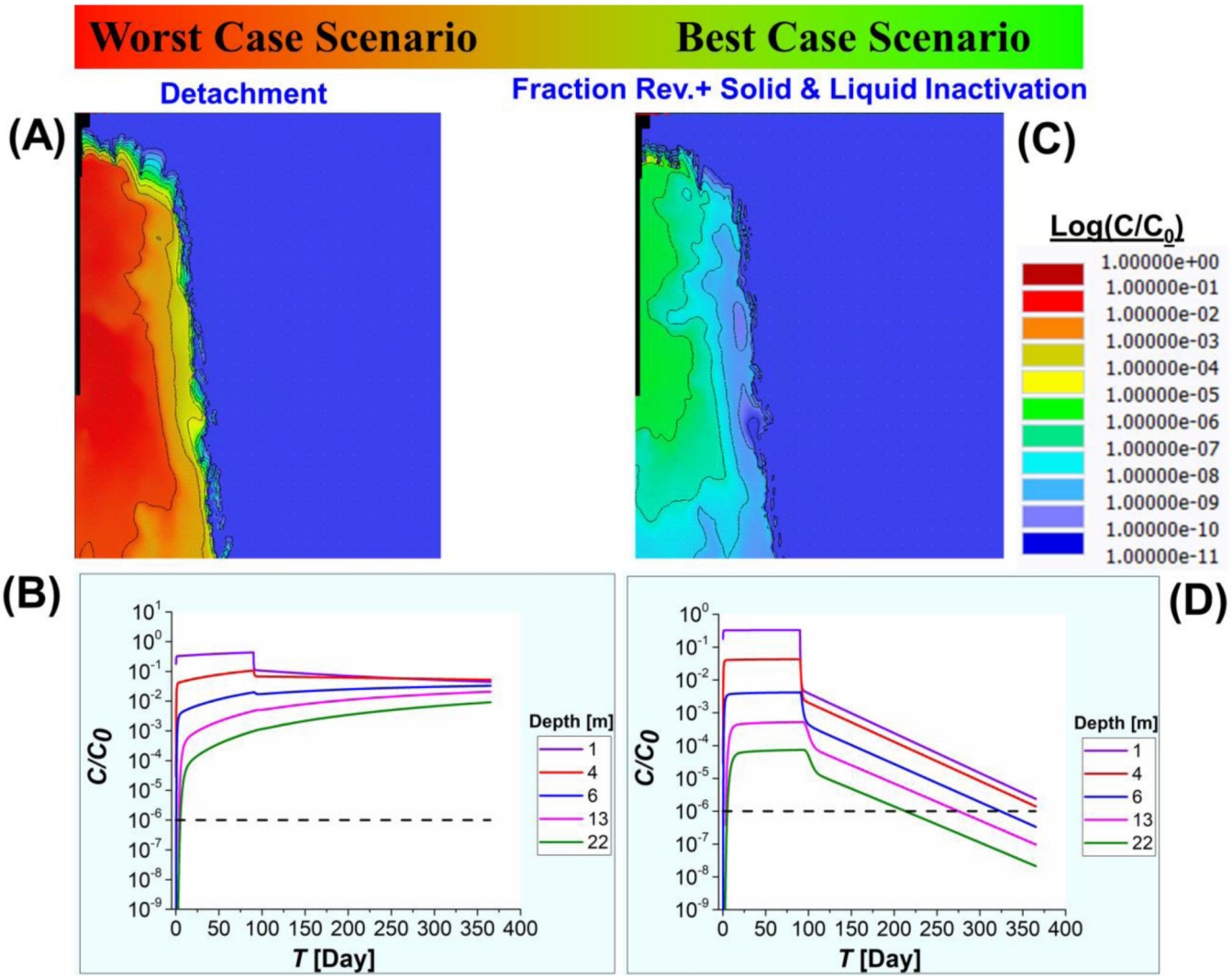

Fig. 7.

The virus concentration distribution for the worst-case (*detachment*) **(A)** and best-case (*reversible fraction* + μ_s + μ_l) **(C)** removal scenarios in the "X=1, Z=2, and σ=1" flow domain. The virus breakthrough curve at depths=1, 4, 6, 13, and 22 m in the "X=1, Z=2, and σ=1" flow domain for the worst-case **(B)** and best-case **(D)** removal scenarios.

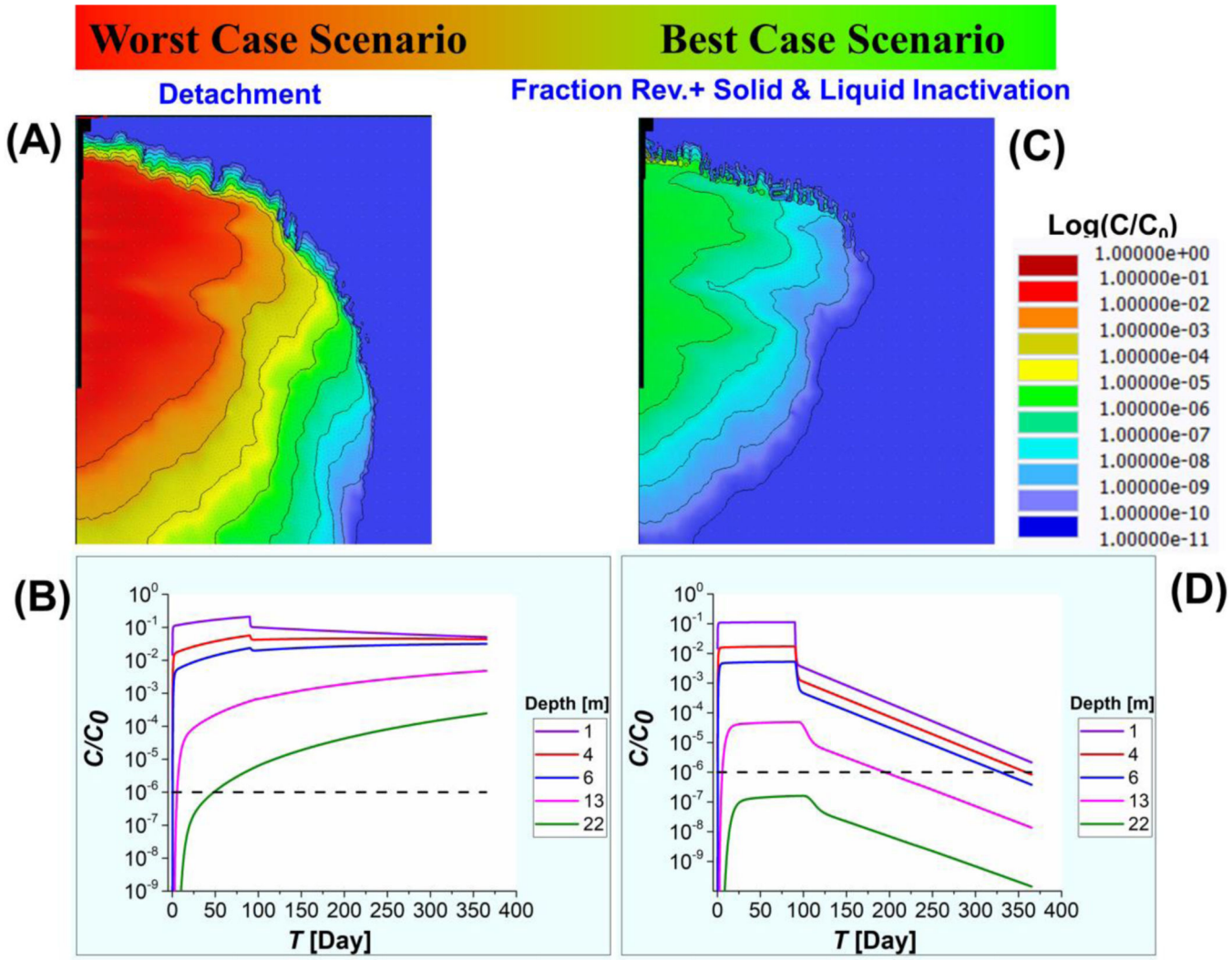

Fig. 8.

The virus concentration distribution for the worst-case (*detachment*) **(A)** and best case (*reversible fraction* + μ_s + μ_l) **(C)** removal scenarios in the "X=10, Z=0.1, and σ=1" flow domain. The virus breakthrough curve at depths=1, 4, 6, 13, and 22 m in the "X=10, Z=0.1, and σ=1" flow domain for the worst-case **(B)** and best-case **(D)** removal scenarios.

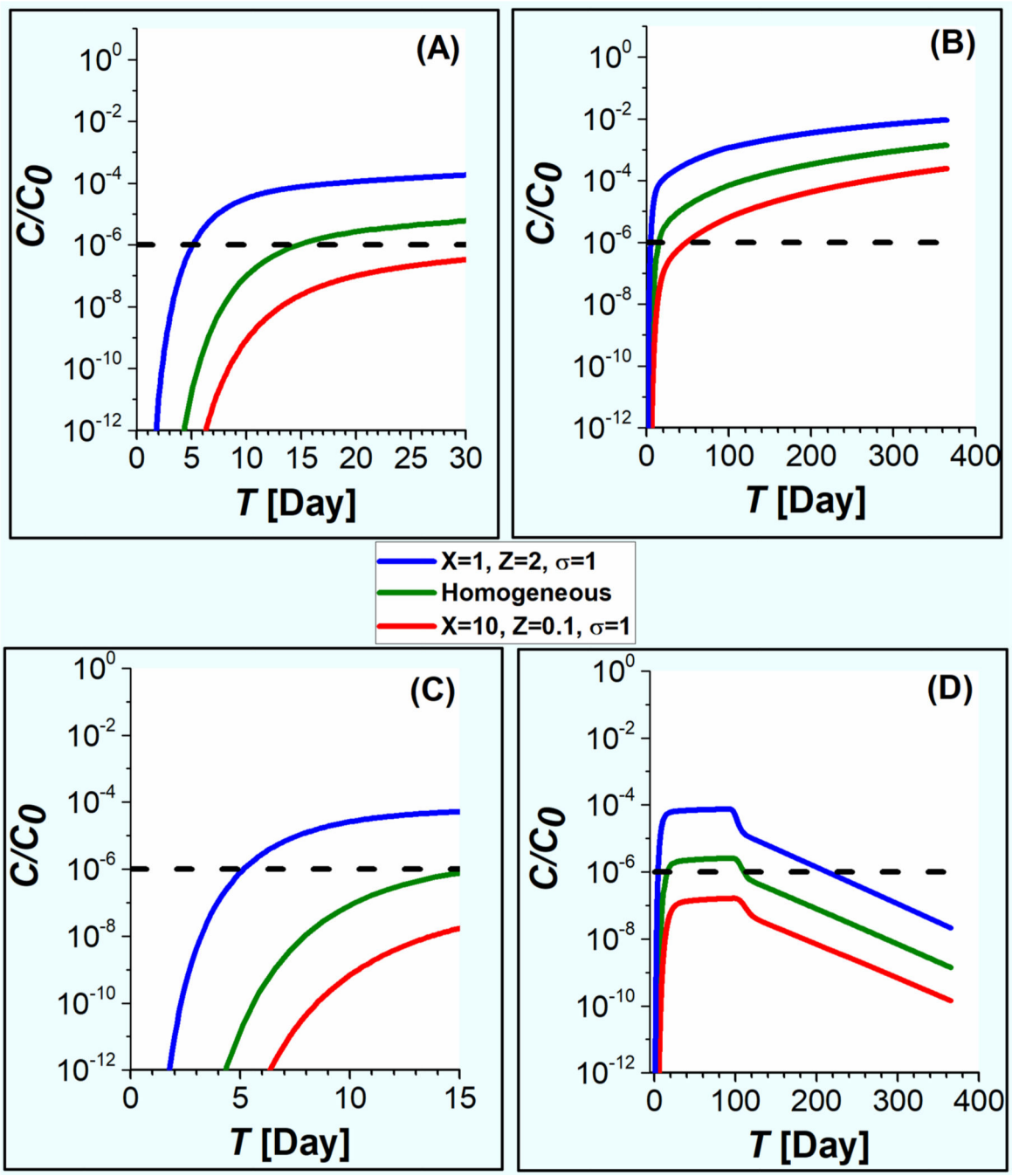

Fig. 9.

The virus breakthrough curves for the worst-case (*detachment*) removal scenario at 22 m as a function of time during 30 days **(A)** and 365 days **(B)**. The virus breakthrough curves for the best-case (*reversible fraction* + $\mu_s + \mu_l$) removal scenario at 22 m as a function of time during 15 days **(C)** and 365 days **(D)**.

Table 1.

The virus removal parameters employed in the numerical experiments and the corresponding flow domains and scenarios.

Experiment	Flow Domain	Scenario	* α	* k_d	* μ_l	* μ_s	* f_r	* $(1-f_r)$
Set IA	Homogeneous	*Irreversible Attachment* $[(f_r=0)+\alpha]$	0 1×10^{-5} 1×10^{-4} 1×10^{-3}	0	0	0	0	1
Set IB			0.47 0.03	0	0	0	0	1
Set II	Homogeneous	*Detachment* $[(f_r=1)+\alpha+k_{d1}]$	1×10^{-4}	1×10^{-5}	0	0	1	0
		Liquid Inactivation $[(f_r=1)+\alpha+k_{d1}+\mu_l]$	1×10^{-4}	1×10^{-5}	1×10^{-5}	0	1	0
		Solid-Phase Inactivation $[(f_r=1)+\alpha+k_{d1}+\mu_l+\mu_s)]$	1×10^{-4}	1×10^{-5}	1×10^{-5}	1×10^{-5}	1	0
		Reversible Fraction $[(f_r=0.1)+\alpha+k_{d1}]$	1×10^{-5}	1×10^{-5}	0	0	0.1	0.9
		Reversible Fraction + $\mu_l[(f_r=0.1)+\alpha+k_{d1}+\mu_l]$	1×10^{-5}	1×10^{-5}	0	1×10^{-5}	0.1	0.9
		Reversible Fraction + $\mu_l+\mu_s[(f_r=0.1)+\alpha+k_{d1}+\mu_l+\mu_s]$	1×10^{-5}	1×10^{-5}	1×10^{-5}	1×10^{-5}	0.1	0.9
Set III	X=10, Z=0.1, σ=1	*Detachment* $[(f_r=1)+\alpha+k_{d1}]$	1×10^{-4}	1×10^{-5}	0	0	1	0
	X=1, Z=0.1, σ=1							
	X=0.1, Z=0.1, σ=1							
	X=1, Z=1, σ=1							
	X=1, Z=2, σ=1							
	X=1, Z=0.1, σ=0.5							
	X=1, Z=0.1, σ=0.25							
Set IV	X=10, Z=0.1, σ=1	*Detachment* $[(f_r=1)+\alpha+k_{d1}]$	1×10^{-4}	1×10^{-5}	0	0	1	0
	X=1, Z=2, σ=1							
	X=10, Z=0.1, σ=1	*Reversible Fraction* + $\mu_l+\mu_s[(f_r=0.1)+\alpha+k_{d1}+\mu_l+\mu_s]$	1×10^{-5}	1×10^{-5}	1×10^{-5}	1×10^{-5}	0.1	0.9
	X=1, Z=2, σ=1							

*sticking efficiency (α), solid-phase inactivation (μ_s), liquid-phase inactivation (μ_l), detachment coefficient (k_d), a reversible fraction (f_r), an irreversible fraction ($1-f_r$)

Table 2.

The PRD1 virus removal parameters used in numerical experiments Set VA and Set VB, corresponding flow domains, and the separation distance to obtain 6-$\log_{10}$ virus removal.

Experiment	**Input Parameters**					**Stochastic Heterogeneity**	**Separation distance for 6-$\log_{10}$ removal**
Reference	* α	* μ_s	* μ_l	* k_{d1}	* k_{d2}		**[m]**
	[−]	[min^{-1}]	[min^{-1}]	[min^{-1}]	[min^{-1}]		
Set VA (Sasidharan et al. 2018b) *(Column Scale Experiment)*	8.1×10^{-2}	4.2×10^{-5}	1.6×10^{-6}	4.8×10^{-8}	1.0×10^{-12}	Homogeneous	1
						X=10, Z=0.1, σ=1	1
						X=1, Z=2, σ=1	1.8
Set VB (Schijven et al. 1999) *(Field Scale Experiment)*	8.6×10^{-4}	4.7×10^{-5}	8.3×10^{-5}	1.7×10^{-8}	NA	Homogeneous	6.5
						X=10, Z=0.1, σ=1	6.8
						X=1, Z=2, σ=1	7.9

* sticking efficiency (α), solid-phase inactivation (μ_s), liquid-phase inactivation (μ_l), detachment coefficient for site 1 and site 2 (k_{d1} and k_{d2})